Quantification of root water uptake distribution of winter barley using water stable isotopes under field conditions

Françoise Vanoverbeke

TRAVAIL DE FIN D'ÉTUDES PRESENTÉ EN VUE DE L'OBTENTION DU DIPLOME DE MASTER BIOINGENIEUR EN SCIENCES ET TECHNOLOGIE DE L'ENVIRONNEMENT

Academic Year 2017-2018

Co-Supervisors:
Prof. Sarah Garré
Prof. Youri Rothfuss

[1] Dans ce cas, l'autorité académique est représentée par les promoteurs membres du personnel enseignant de GxABT.

Quantification of root water uptake distribution of winter barley using water stable isotopes under field conditions

Françoise Vanoverbeke

TRAVAIL DE FIN D'ÉTUDES PRESENTÉ EN VUE DE L'OBTENTION DU DIPLOME DE MASTER BIOINGENIEUR EN SCIENCES ET TECHNOLOGIE DE L'ENVIRONNEMENT

Academic Year 2017-2018

Co-Supervisors:
Prof. Sarah Garré
Prof. Youri Rothfuss

Remerciements

Tout d'abord, je tiens à remercier tout particulièrement mes promoteurs Youri Rothfuss et Sarah Garré sans qui ce travail n'aurait pu aboutir. Je tiens à vous remercier pour votre grande disponibilité, votre écoute, vos avis d'experts scientiques, ainsi que pour la liberté que vous m'avez accordée durant ces six derniers mois. Merci également pour la bienveilance que vous avez eue à mon égard lors de ma chute en vélo.

Merci à Gilles Colinet de m'avoir permis l'utilisation de matériel technique, ainsi que d'avoir mis un laboratoire à ma disposition. Merci à Félix pour avoir partagé ses connaissances pédologiques.

Merci à toute l'équipe de l'axe Echange Eau-Sol-Plante, merci à Stéphane Becquevort et Gilles Swerts pour votre précieuse aide technique sur le terrain. Merci à Katia, à NJaka pour m'avoir montré le fonctionnement de l'Hyprop, et à Sid pour la relecture ainsi que les pauses au soleil dans le parc. Merci également à mes camarades Thib, Cédou et Guigui sans qui l'ambiance conviviale n'aurait pas été la même.

Merci à tous mes ami.e.s, co-kotteurs pour vos sourires et vos encouragements.

Un merci tout spécial à ma Maman grâce à qui j'ai eu la chance de réaliser ces longues études. Merci pour ton soutien et l'amour que tu m'as apportés.

Enfin, merci à Gilles, pour tout.

"The specific sensitivity of isotopes during phase changes or reactions can be exploited to track changes in the environment" [Macaigne, 2011].

Abstract

From carbon dating to hydrology, isotopic approaches have a wide range of applications, such as the study of climate change or nutrients cycling in soils. Water stable isotopic analysis is also a promising tool to better understand water dynamics in soil since it can be used to trace root water uptake at different depths.

This MSc thesis had two objectives: one technical and one scientific. The first technical objective was a proof of concept in the field of a novel soil water vapour extraction method. This method had already been tested and calibrated in laboratory by Rothfuss et al. which considers isotopic thermodynamic equilibrium between soil liquid water and soil water vapour and the unique requirement of a temperature correction. The second scientific objective was the determination of the vertical root water uptake profile of winter barley crops from isotopic information. This has been done via a multi-sources mixing model (SIAR) that confronts stable isotopic compositions of soil water across depth, with stable isotopic compositions of crop xylem sap water.

From a technical aspect, the gas-permeable tubing method is working properly in the field. It provides enough water quantities to be analysed off-line with a laser spectrometer. This study however outlines fractionation errors during the sampling.

This work provides insight into RWU patterns of winter barley for its last stage development. Furthermore, this study underlines the importance of input data when using multi-sources mixing model. The sources isotopic signatures have to be discriminative so that the model can differentiate them. Extra parameters such as the root length density and soil water content are essential to provide thorough results.

Keywords: Water stable isotopes, root water uptake, Hordeum vulgare L., SIAR, soil water vapour extraction, gas permeable tubing.

Résumé

De la datation au carbone à l'hydrologie, les approches isotopiques ont un large éventail d'applications, telles que l'étude des changements climatiques ou du cycle des nutriments dans les sols. L'analyse isotopique stable de l'eau est également un outil performant permettant de mieux aborder des phénomènes complexes, tels que l'absorption d'eau par les racines à différentes profondeurs.

Ce mémoire avait deux objectifs: un technique et un scientifique. Le premier objectif technique était une preuve de concept dans le domaine d'une nouvelle méthode d'extraction de la vapeur d'eau dans le sol. Cette méthode avait déjà été testée et calibrée en laboratoire par Rothfuss et al. Son travail a permis de considérer l'équilibre thermodynamique isotopique entre l'eau liquide du sol et la vapeur d'eau du sol et l'exigence unique d'une correction de la température. Le second objectif scientifique consistait à déterminer le profil d'absorption verticale de l'eau des racines des cultures d'orge d'hiver à partir des données isotopiques. Ceci a été fait via un modèle de mélange multi-sources (SIAR) qui confronte les compositions isotopiques stables de l'eau du sol à travers les profondeurs, avec des compositions isotopiques stables d'eau de sève de xylème de la culture à la base du premier noeud de l'orge.

D'un point de vue technique, la méthode des tubes perméables aux gaz a fait ses preuves sur le terrain. Elle a fourni des quantités d'eau suffisantes permettant leur analyse avec un spectromètre au laser. Cette étude a cependant mis en évidence des erreurs de fractionnement lors de l'échantillonnage.

Ce travail a permis d'identifier les profils de prises d'eau racinaires de l'orge d'hiver pour son dernier stade de développement. En outre, cette étude a souligné l'importance des données d'entrée lors de l'utilisation du modèle de mélange multi-sources. Les signatures isotopiques des sources doivent être discriminantes pour que le modèle puisse les différencier et fournir en retour des résultats plausibles. Des paramètres supplémentaires tels que la densité de longueur des racines et la teneur en eau du sol sont essentiels pour obtenir des résultats complets.

Mots-clefs: Isotopes stables de l'eau, prise d'eau racinaire, Hordeum vulgare L., SIAR, extraction de la vapeur d'eau du sol, tubes perméables aux gaz.

Contents

1 Introduction **1**

2 State of the art **3**

2.1 Water stable isotopes: definitions and terminology . . . 3

2.1.1 Definitions . . . 3

2.1.2 International reference . . . 4

2.1.3 Water stable isotopic fractionation . . . 4

2.2 Water stables isotopes during phase changes . . . 7

2.2.1 Isotopic fractionation in the environment . . . 7

2.2.2 Relationship between $\delta^2 H$ and δ^{18}O . . . 8

2.2.3 Soil evaporation (Barnes and Allison) . . . 9

2.3 Root Water Uptake . . . 11

2.3.1 Definitions . . . 11

2.3.2 Main drivers of the RWU process . . . 11

2.3.3 Available water . . . 12

2.4 Link between isotopes and RWU . . . 13

2.4.1 Hypotheses . . . 13

3 Materials and methods **15**

3.1 Experimental site . . . 15

3.1.1 Study site . . . 15

3.1.2 Soil profile . . . 16

3.1.3 Crop and technical itinerary . . . 18

3.1.4 Soil water retention curves . . . 18

3.2 Soil water vapour extraction method . . . 20

3.2.1 Application of the method . . . 20

3.2.2 Description and functioning of the method . . . 22

3.2.3 Field experimental setup . . . 24

3.3 Sampling of the xylem water . . . 26

3.4 Measure timing . . . 26

3.5 Soil moisture and temperature monitoring . . . 27

3.6 Root Length Density measurements . . . 28

3.6.1 Soil sampling . . . 28

3.6.2 Roots washing . . . 28

3.6.3 Roots scan . . . 29

3.6.4 Image analysis . . . 29

3.7 Determination of RWU profiles with statistical modeling . . . 31

3.7.1 Model input . . . 31

3.7.2 Model run . . . 31

3.7.3 Model outputs . . . 32
3.7.4 Model priors . . . 33

4 Results **34**
4.1 Soil water vapour extraction: quantitative outcomes . . . 35
4.2 Environmental parameters . . . 37
4.3 Prior information in the model: RLD and SWC . . . 39
4.3.1 Evolution of volumetric soil water content with time and depth 39
4.3.2 Evolution of the Root Length Density with depth . . . 40
4.4 Variation of $\delta^2 H$ and δ^{18}O, temperature, soil moisture content and potential with depth . . . 41
4.5 Dual isotope plot . . . 43
4.6 RWU profiles using SIAR . . . 45
4.6.1 No prior information in the model . . . 45
4.6.2 Prior information in the model . . . 46
4.6.3 SWC and pF evolutions through depth and time . . . 48

5 Discussion **50**
5.1 Evaluation of the method of soil water vapour extraction from the soil 50
5.1.1 Viability of the system deployed in the field . . . 50
5.1.2 Logistical considerations . . . 50
5.2 Evaluation of the method of soil water extraction from the traps . . . 51
5.3 Challenges, limitations and advantages of the method . . . 53
5.4 Retrieving relative RWU profiles of winter barley . . . 53
5.4.1 Model inputs . . . 54
5.4.2 Model outputs . . . 54
5.4.3 Ecological interpretations . . . 55

6 Outlook **57**

7 Conclusion **58**

References **59**

A Appendix **65**
A.1 List of symbols . . . 65
A.2 List of acronyms . . . 65
A.3 Field and lab protocols . . . 65
A.4 Calibration equations for the 5TM probes . . . 68
A.5 Calculation of the p_j's standard deviation . . . 69
A.6 Pictures . . . 70
A.6.1 Tubing installation in the field . . . 70
A.6.2 Extraction line of the Jülich laboratory . . . 71

A.7 Output data of the model SIAR 71

List of Figures

1 Schematic representation of fractionation stable water isotope due to several processes in natural environment ("+" signs represent enrichment, "-" signs depletion and "O" neither enrichment or depletion) [Sprenger et al., 2016]. 7
2 Relationship between $\delta^2 H$ and δ^{18}O for ocean waters (0,0) and for meteoric waters represented by the Global Meteoric Water Line [Gat et al., 2001]. 9
3 Soil water isotopic composition δ_s with respect to depth (z), according to Barnes and Allison [Allison et al., 1983, Rothfuss and Javaux, 2017]. "EF" represents the "Evaporation Front". 10
4 Theoretical retention function for a sandy-clay soil [Degré, 2017]. . . . 12
5 Localisation of the agroforestery field east of Gembloux Agro-Bio Tech. The field is represented by a blue frame and the exact location of the experiment by a black cross (Google Earth). 15
6 Picture of the site one week after the installation of the underground material needed for the experiment. 16
7 Picture of the soil profile with the three horizons represented. 17
8 Retention curves obtained with Hyprop for three soil samples corresponding to the following depths: 10, 40 and 100 cm. 19
9 The left picture shows a soil sample water (extracted at 20 cm) in the trap. Condensation can be seen on the rim of the trap. The left picture shows the temperature gradient made with a hotgun (blowing air at 250°C) in the upper part and dry ice in the lower part. 21
10 Different steps of the liquid soil water extraction from the trap: variant of the method presented by Rothfuss et al. The green part is the field part while the gray part represents the laboratory part. 22
11 Design and picture of the dry ice making in order to cool the soil water vapour and force condensation of water vapour extracted. . . . 24
12 Design of the soil water extraction device in the field. 24
13 Design of the soil water extraction device in the field. This schematic representation shows the device for one tube. The red cross indicates the position of the 5TM soil moisture and temperature probes. 25
14 Schematic design of the plant's sampling zone, located in the white frames. 26
15 The left picture shows the soil cores that are sampled manually with an auger in the field. The right picture shows the device to separate and wash the roots from the soil samples. 28
16 Selection and extend of the roots before the scan in a water solution. 29

17 Example of transformed and analysed image with ImageJ; the left picture is a scan of the roots and the right picture is the same image after treatments. 30
18 Soil water volume harvested at each depth for the last four dates of experiment (Date 5, Date 6, Date 7 and Date 8). The color gradient indicates the measured incoming dry air flow before each cold trap. . 35
19 Soil and air temperature conditions and their evolution through time. 37
20 Evolution of precipitations (in mm) and relative humidity (in %) through time. The red diamonds localise the eight experiments in time. 38
21 Soil volumetric water content measured by the 5TM probes and its spatial and time evolution. 39
22 Variation of the RLD in (cm cm^{-3}) through depth with the respective standard deviation. 40
23 Evolution of soil temperature, volumetric water content, plant and soil water isotopic composition through depth for each time step. . . . 41
24 Dual isotope plot: relationship between $\delta^2 H$ and δ^{18}O for each soil water samples and xylem sap water sample (plants) represented for each experimentation date. The different symbols represent each corresponding soil depth at which soil water samples have been extracted. 43
25 Most frequent RWU proportion and its evolution through depth and time without prior insert in the model. Values of plant standard deviation for δ_{ti} were equal to $\pm$ 1 or 2 ‰ (for O or H respectively) (left plot) and of $\pm$ 0.1 or 0.2 ‰ (for O or H respectively) (right plot), as well as analytical standard deviation values (less than 0.07‰ for O and less than 0.5‰ for H) concerning δ_s for both plots. 45
26 Most frequent RWU proportion and its evolution through depth and time without prior insert in the model for δ_{ti} plant standard deviation of $\pm$ 1 or 2‰ (left plot) and of $\pm$ 0.1 or 0.2‰ (right plot), and with a value of standard deviation of $\pm$ 1 or 2‰ for δ_s for both plots. . . . 46
27 Most frequent RWU proportion and its evolution through depth and time with RLD and SWC used as prior information in the model. This graph results from different standard deviation inserted in the model: $\pm$ 1 or 2 ‰ or $\pm$ 0.1 or 0.2 ‰ for δ_{ti} and $\pm$ 1 or 2 ‰ or analytical errors for δ_s. 47
28 Value of p_j, the prior vector for each time calculated on the base of equation (18). 48
29 Evolution of the SWC (left plot) and of pF values (right plot) through depth and time, considering each experimentation date. 49

30 Comparison of the trap just after the field extraction (left picture) and after the laboratory part with the hotgun (right picture). Evidence of water mobilisation at the bottom of the trap is visible. 52
31 Evolution of the volumetric water content with the dielectric permittivity (ε_0, the raw output data of the sensor) and their respective fit calculated via the model "CurveExpert Basic®"). 68
32 Pictures of the tubing installation. Left picture shows the tubes installed 1.3 m deep while the right picture shows the installation at 0.2 m. 70
33 Picture of the extraction line of Jülich Forschungszentrum. 71

List of Tables

1 Stable isotopes of hydrogen and oxygen with their respective atomic number, neutrons number and mass number, as well as their natural abundance in % [Gat et al., 2001] 3
2 The depth, a brief description and the soil bulk densities are given with respect to the soil horizon. 18
3 Agricultural practices according to the date. 18
4 5TM sensor depths and matching horizon. 27
5 The dates of the experiments, their day in the year, the main cereal development stage, the stage number referred by the BBCH scale, as well as the extraction time. 34
6 Isotopic composition in precipitaitons of ^{2}H and ^{18}O (corrected with the SMOW) for the specific location of the experiment, according to Bowen [Bowen G. J. and A., 2005]. 42
7 Linear regression's slope, intercept, R^2 and p-value of the regressions concerning the 5 δ_s of each date, as well as in the last line, concerning δ_{ti} of all dates. 44

1 Introduction

Agriculture is responsible for sixty percent of water use in the world. As more and more land is at risk of facing water scarcity in the context of climate change, there is a need for deeper knowledge on crop's water use [Horrigan et al., 2002, Vandoorne et al., 2012]. A deeper understanding of the spatial and time variation of the Root Water Uptake (RWU) is essential in a view of for example better manage irrigation plans, but also to answer ecological questions around plant and/or tree competition and to a certain extent to get insights on the way to design intercropping systems [Dawson et al., 2002, Rothfuss and Javaux, 2017].

Water stable isotopes analysis has recently enhanced the grasp we have about water uptake processes by vegetation simply because isotopic compositions of different water sources (δ^2H and δ^{18}O) are differenciable [Gat, 1996, Dawson et al., 2002]. The contribution of isotopic approaches to address hydrological issues is becoming more and more significant [Bowen et al., 2007]. In 2016, Sprenger et al. reviewed the use of water stable isotopes in research on hydroglogical processes [Sprenger et al., 2016]. In 2017, Rothfuss and Javaux focused on ways to quantify RWU by plants using water stable isotopes. It has been fifteen years that the water stable isotopes are used to localise the RWU [Rothfuss and Javaux, 2017]. Isotopic approach provides a way to shed light on the soil-plant-water relationships and particularly the RWU, which is quite challenging to quantify [Ogle et al., 2004]. The RWU, is mainly governed by transpiration process, but also affected by "the root system distribution, the soil hydraulic properties, and the climatic conditions" [Yu et al., 2007].

Water stable isotope measurements also have limitations, which are mostly related to destructive sampling and offline isotopic analysis leading to low spatial and temporal resolutions of the isotopic compositions data. The need to improve in situ advanced techniques for soil and xylem water extraction with a high time and spatial resolution has been pointed out in the literature [Stumpp et al., 2018, Orlowski et al., 2016]. The aim is to increase both data precision and our understanding of ecohydrological phenomenons [Stumpp et al., 2018]. Recently, a novel non-destructive and minimally invasive method with permanent harvesting tubes in the soil profile has been developed. The method allows the monitoring of the isotopic compositions of soil water and transpiration fluxes [Rothfuss et al., 2013, Rothfuss et al., 2015]. While it provides mean to increase the temporal resolution of isotopic data series, it also requires expensive measurement systems (e.g. in situ laser spectrometer). In the present study, we propose a compromise between i. the determination of soil liquid water isotopic composition based on a non-destructive sampling (i.e., with gas permeable tubing) and ii. an offline isotopic analysis in the laboratoy by trapping soil water vapor cryogenically in the field. This cost-effective variation of the iso-

topic method of Rothfuss et al. (2013) does not rely on the use of an in situ laser spectrometer and could be, once successfully validated, an alternative to the widely used destructive isotopic methods.

Objectives

The objectives of this MSc thesis are therefore both technical and scientific: i) to establish a proof-of-concept for the soil water vapour extraction in the field; and (ii) to use this method to determine the vertical root water uptake profile of winter barley using water stable isotopes.

In this work we tested the following hypotheses: i.1) Enough soil water vapour can be harvested under field conditions to measure the isotopic composition. i.2) Field and laboratory extraction is sufficiently rigorous to avoid problems of contamination during the extraction of the soil water vapour. ii.1) Using the Stable Isotopes Analysis model in R (SIAR) in combination with values of stable isotopic compositions of crop xylem sap and soil water at different depths, we can determine the root water uptake vertical profile of winter barley in the field at different time steps. ii.2) The result of this root water uptake profile can be improved using Root Length Density data and soil moisture data.

2 State of the art

2.1 Water stable isotopes: definitions and terminology

2.1.1 Definitions

Hydrogen and oxygen atoms which are the constituants of water (H_2O) can naturally occur under the form of stable isotopes. The "isotopes" are the atoms of a chemical element which have the same number of protons but have a variable number of neutrons. The atomic number of an atom is defined by its number of protons (Z) while the mass number (A) is equal to the number of neutrons and protons [Kotz and Treichel Jr, 2006] (figure 1). The term "stable" is used because it refers to the "non radiactive" dimension of the element, meaning that there is no disintegration over time [Macaigne, 2011]. For that reason, stable isotopes are safe to handle, which is more convenient compared to the radioactive ones [Smit et al., 2013].

The heavier stable isotope of oxygen (^{18}O) has two additional neutrons and the stable isotope of hydrogen, called deuterium (^2H or ^2D) has one neutron in its nuclei. These configurations confer a bigger mass to the isotopes. The mass is twice bigger for deuterium compared to hydrogen and ^{18}O is 12.5% heavier than ^{16}O. This mass difference alters the isotope's involvement in chemical reactions such as phase changes. For example, heavy water (enriched in isotopes) will be less preferentially involved in the evaporation reaction. This situation leads to an accumulation of heavier water stable isotopes in the remaining water liquid phase [Sprenger et al., 2016].

Element	Atomic number (Z)	Neutrons number (N)	Mass number (A)	Abundance (%)	Symbol
Hydrogen	1	0	1	99.985	^1H
	1	1	2	0.00159	^2H
Oxygen	8	8	16	99.759	^{16}O
	8	9	17	0.037	^{17}O
	8	10	18	0.204	^{18}O

Table 1: Stable isotopes of hydrogen and oxygen with their respective atomic number, neutrons number and mass number, as well as their natural abundance in % [Gat et al., 2001]

The two stables isotopes of hydrogen (^2H and ^1H) and the three ones of oxygen (^{18}O, ^{17}O and ^{16}O) (Figure 3.) statistically imply the presence of nine possible molecules of water. The latter are called isotopologues of water. However, only

$^1H^1H^{16}O$, $^1H^1H^{18}O$ and $^1H^2H^{16}O$ are actually quantifiable with a valid accuracy [Rothfuss, 2017].

It is possible to measure the isotopic abundances in the environment and to quantify water stable isotopes through the use of Isotope Ratio Mass Spectroscopy (IRMS) or Isotope Ratio Infrared Spectroscopy (IRIS). These measurement systems are able to give the isotopic abundance ratio, R, which is a concentration ratio,

$$^iR = \frac{C_i}{C_{^1H_2{}^{16}O}}, \tag{1}$$

with i = $^1H^2H^{16}O$ or $^1H^1H^{18}O$. The water isotopic composition (δ) is generally used instead of using directly the R ratio. The δ is defined regarding the SMOW (Standard Median Ocean Water) reference:

$$\delta = \frac{^iR_{sample} - ^i R_{ref}}{^iR_{ref}}, \tag{2}$$

and is expressed in permil (‰) units because it is naturally present in small quantities. The reference water standard (R_{ref}) is given in order to determine isotopes in a relative scale [Hagemann et al., 1970].

2.1.2 International reference

The ocean water is the reference for both hydrogen and oxygen isotopic compositions because it is the biggest reservoir and is considered as quite uniform [Gat, 1996] [Craig, 1961]. In this context, it is possible to classify two kinds of water: the ocean water and the meteoric waters (for example, evaporating water, air moisture, precipitations, ground and surface water). Meteoric waters have the characteristic to be depleted in ^{18}O and ^2H. Hence almost every isotopic value are negative, because always compared to the ocean water which is conventionally neither depleted or enriched in heavy isotopes [Gat et al., 2001]. It is therefore commonly stated that:

$$\delta^{18}O_{SMOW} = 0‰ \text{ and } \delta^2H_{SMOW} = 0‰. \tag{3}$$

2.1.3 Water stable isotopic fractionation

The natural disparity of isotopes in the environment reflects the sensitivity of stable isotopes to react differently in reactions. The changes in the isotopic composition of an element are what we call the "fractionation process". The mass difference induced by the extra neutrons changes the molecule's physical and chemical properties. This leads to a change in the R concentrations ratio between light and heavy isotopes and therefore to a fractionation effect [Mook and Rozanski, 2000, Sprenger et al., 2016].

Firstly, the heavier the isotope, the smaller its velocity. It can be explained by the kinetic equation, which is :

$$kT = \frac{m \cdot v^2}{2} \tag{4}$$

with k, the Boltzmann constant and T the temperature, m is the molecular mass and v is the average molecular velocity. At a given temperature, the right side of the equation is also constant. Therefore, if the mass of a molecule is higher, its average velocity will be lower. These heavier molecules have consequently a lower reaction velocity compared to lighter ones. One of the consequences is that the risk of collision, needed for chemical reaction, decreases.

Secondly, the heavier the atoms, the harder it is to break the bonds between them because it requires a higher activation energy to overcome the attractive force.

As a result, the vapour pressure of isotopic water, composed of ^2H or ^{18}O, is lower than the one of water composed of ^1H and ^{16}O [Mook and Rozanski, 2000].

The effect of temperature has a role to play in the isotope effect: as the temperature gets higher, the isotope effect decreases. Indeed, the temperature decreases the binding energy between atoms but also decreases the activation energy necessary to break the bonds. This makes it easier for a chemical reaction to take place. Hence, the isotopic effect at equilibrium is temperature dependent [Mook and Rozanski, 2000].

In general, the fractionation ($\varepsilon_{B/A}$) is used in order to reflect the depletion or the enrichment of heavy isotopes in a sample between two phases (from A to B). It derives from the fractionation factor ($\alpha_{B/A}$) through the relation

$$\varepsilon_{B/A} = \alpha_{B/A} - 1 = \frac{R_B}{R_A} - 1. \tag{5}$$

It is important to draw a distinction between to two types of fractionation: the kinetic and the equilibrium fractionation, which affect differently the fractionation factor [Mook and Rozanski, 2000].

In the **equilibrium fractionation**, the isotopic effect occurs at chemical equilibrium and can be described as a reversible exchange reaction. For example in the case of a phase change between liquid and vapour:

$$H_2^{16}O_{liquid} + H_2^{18}O_{vapour} \leftrightharpoons H_2^{16}O_{vapour} + H_2^{18}O_{liquid} \tag{6}$$

In this case, the equilibrium constant equals the fractionation factor:

$$K = \alpha^*_{B/A}. \tag{7}$$

The equilibrium state in a case of phase change (liquid-vapour) can be characterized by a closed system where there is a hundred percent of humidity and a steady temperature [Sprenger et al., 2016]. In soils, water vapour is considered in equilibrium state with the liquid phase [Soderberg et al., 2012]. The thermodynamic equilibrium describes a situation where there is as much as water that condensates that it evaporates. In other words, "a dynamic exchange of water molecules occur without leading to a visible change" [Gat, 2010].

In 1971, Majoube found the relationship between the fractionation factor (in a case of water phase change) and the temperature for an equilibrium state,

$$1000 \cdot \ln \alpha = C_1 + \frac{C_2 10^3}{T} + \frac{C_3 10^6}{T^2}. \tag{8}$$

This equation holds for temperature from 273,15 to 373,15 K. C_1, C_2 and C_3 are coefficient that are experimentally determined for ^{2}H and ^{18}O [Majoube, 1971].

Kinetic fractionation, on the other hand, results from a phase change, for instance between the liquid and the vapour state of water. In other words, a change in equilibrium of phase-change reactions or a unidirectionnal reaction, shapes the isotopic composition of water [Bowen et al., 2007]. Kinetic fractionation also plays a key role in the natural variation of both hydrogen and oxygen isotopic compositions. In order to distinguish the kinetic fractionation factor from the equilibrium one, we generally use the α_k, defined as

$$\alpha_k = \frac{R_B}{R_A}, \tag{9}$$

where A and B refer to different phases. In this case, the system is open and there is an "outgoing" flux of water with a different isotopic signature [Gat, 1996].

Fractionation is a prevailing and fundamental process acting all along this field and laboratory experiment. This process makes the differentiation between different isotopic signature possible and the ability to use water as a tracer, because water is carrying out this information in the environment.

2.2 Water stables isotopes during phase changes

2.2.1 Isotopic fractionation in the environment

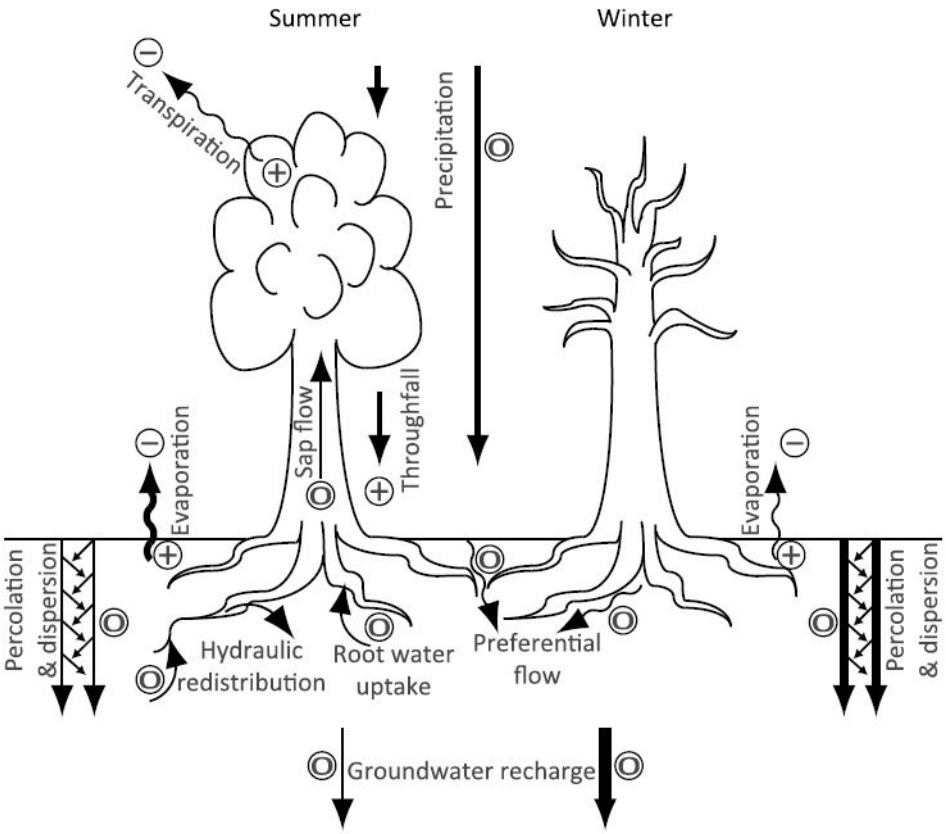

Figure 1: Schematic representation of fractionation stable water isotope due to several processes in natural environment ("+" signs represent enrichment, "-" signs depletion and "O" neither enrichment or depletion) [Sprenger et al., 2016].

In the light of hydrological processes at the soil-vegetation-atmosphere continuum, the main fractionation process is due to evaporation, leading to an enrichment of heavy isotopes in the upper layers of the soil. This situation is described in the figure 1, where "+" signs represent a enrichment and "-" signs a depletion in heavy isotopes. To a smaller extent, throughfall enrich the soil in heavy isotopes. However, its driving processes are less understood. Moreover, the impact of water infiltration variation in space and time on the soil water stable isotopic composition has not yet been clearly evaluated in studies. Duration and intensity of rain events influence on soil water stable isotopic signature. It has a particular depletion effect in heavy isotopes in soil surface [Sprenger et al., 2016].

Water stable isotopes have long been studied in a theoretical framework. Below are presented two examples of models developed by Graig and Gordon and Rayleigh in order to better understand fractionation processes in the environment.

Graig and Gordon model. A conceptual model of isotopic fractionation throughout evaporation from a free water surface has first been proposed by Graig and Gordon in 1965 [Gat et al., 2001]. The model describes water vapour flow in analogy with Ohm's law where the water flow is being divided by a resistance. For the last forty years this model has shown its robustness to predict isotopic effect under various environmental conditions [Horita et al., 2008].

Rayleigh model. Equations of Rayleigh describe a fractionation process under the form of two reservoirs partitioned in isotopes while one of them shrinks in dimensions [Sprenger et al., 2016]. The model supposes that the equilibrium is directly reached and the equilibrium fractionation dominates the relationship between the liquid and the gas in the system. The function described takes the shape of an exponential [Kotz and Treichel Jr, 2006]. This model can theorecally describes a rain event from a cloud (one reservoir is the cloud while the second reservoir is the precipitations). According to Sun et al., under equilibrium state, soil water evaporation is a phenomenon governed by the Rayleigh model [Sun et al., 2009].

2.2.2 Relationship between $\delta^2 H$ and δ^{18}O

It is essential to figure out how the isotopic composition of rainfall water varies in order to understand variations of soil water isotopic signature. Indeed, changes in the isotopic composition of the rain water is another source of isotopic variation in the soil water [Marshall et al., 2007]. In 1961, Harmon Graig showed that there is an average linear relationship between δ^2H and δ^{18}O in rainfall water:

$$\delta^2 H = 8.2 \cdot \delta^{18} O + 11.27‰. \tag{10}$$

This equation line is defined by the global meteoric water line (GMWL) in the dual isotope plot (figure 2) [Craig, 1961]. The line characterises a situation of "equilibrium fractionation", itself described by Rayleigh processes [Sprenger et al., 2016]. An equilibirum state is represented by the node in the figure 2 [Gat et al., 2001].
A deviation of the GMWL is typically observed in a situation of evaporation (see black arrow in the figure 2). This deviation is caused by a decrease in the deuterium excess (will be inferior to 10%), defined as:

$$d_{Excess} = \delta^2 H - 8 \cdot \delta^{18} O. \tag{11}$$

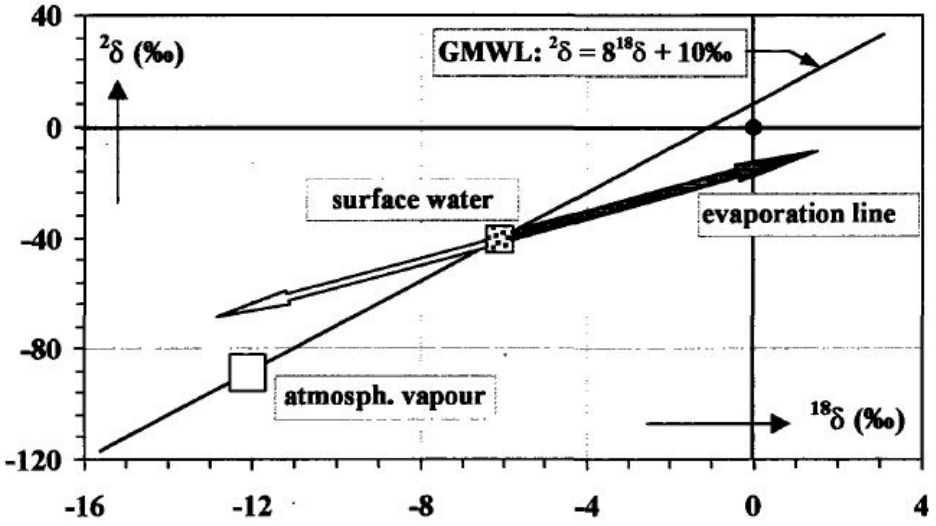

Figure 2: Relationship between $\delta^2 H$ and δ^{18}O for ocean waters (0,0) and for meteoric waters represented by the Global Meteoric Water Line [Gat et al., 2001].

Local Meteoric Water Line (LMWL) can be constructed to describe the same relationship as the GMWL but in a particular region. Indeed, some geographical factors (altitude, latitude and continental effects) influence the water phase changes (cloud and precipitation formation) and therefore play a key role in the rainwater fractionation [Sprenger et al., 2016] [Gat et al., 2001].

Values of δ^2H and δ^{18}O in precipitations of the region of the experiment can be given by An Online Isotopes in Precipitation Calculator (accessible on the website [Bowen, 2018]).

2.2.3 Soil evaporation (Barnes and Allison)

Natural variation of water stable isotopic compositions combined with equilibrium and kinetic fractionation that occur in soil and on its surface during evaporation lead to heavy isotopes enrichment at the soil surface [Gat et al., 2001, Dubbert et al., 2013]. The evolution of $\delta^2 H$ or $\delta^{18} O$ in unsaturated soil water across depth can be divided into two zones. In between those, there is the evaporation front (EF) (dotted blue line in the figure 3). The EF is the depth at which the enrichment in heavy isotopes is the highest in soil. During dry periods, this EF moves towards deeper soil layer. The first zone (above the EF, called the "vapour region" in the figure 3) shows a gradual increase trend : water becomes enriched in heavy isotopes until it reaches the EF. This depletion near the surface is explained by the influence of atmospheric water vapour that diffuses in the soil surface. The second zone is described by a

decreasing exponential shape of the $\delta^2 H$ or $\delta^{18} O$ downward in the soil. The depletion occurs because the kinetic fractionation linked to evaporation progressively decreases through depth [Barnes and Allison, 1988, Yakir and Sternberg, 2000]. On the graph of the figure 3, z represents the depth and "EF" the "Evaporation Front".

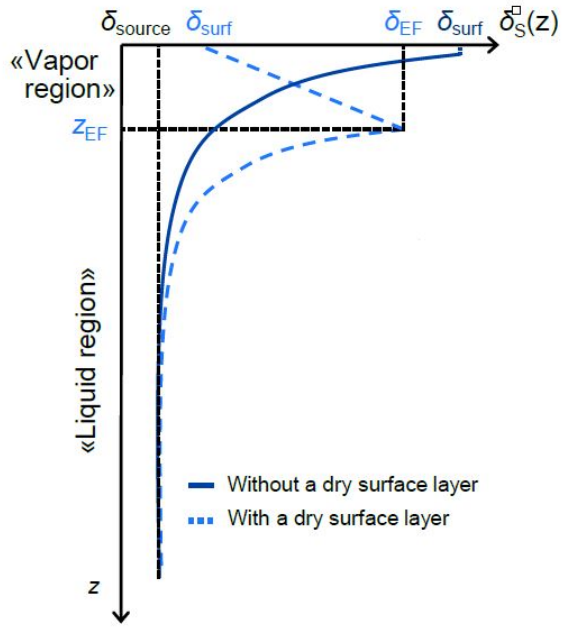

Figure 3: Soil water isotopic composition δ_s with respect to depth (z), according to Barnes and Allison [Allison et al., 1983, Rothfuss and Javaux, 2017]. "EF" represents the "Evaporation Front".

Vegetation impacts the isotopic profile since it acts as a resistance to the evaporation process and consequently decreases the isotopic effect by decreasing the kinetic fractionation [Barnes and Allison, 1988, Sprenger et al., 2016].

2.3 Root Water Uptake

2.3.1 Definitions

Root water uptake (RWU) is defined as "the amount of water abstracted by a root system from soil over a certain period of time", while being at the core of interactions in the water soil plant continuum [Rothfuss and Javaux, 2017]. RWU remains challenging to measure. At the same time, modeling definitly contributes to a better comprehension of the RWU dynamics [Lobet et al., 2014].

2.3.2 Main drivers of the RWU process

Transpiration is the essential physiological process contributing to the RWU. Specifically, "the opening of stomata, the evaporating demand from the atmosphere, the leaf water status and the stress hormonal signals" are the main drivers of the RWU. At the local scale, RWU is driven by the water potential difference between the soil and the roots [Rothfuss and Javaux, 2017]. Water is usually uptaken by the roots where the soil water potential has the least negative value (or maximum), equivalent to the wettest areas. This maximum value can also correspond to large pore areas [Pallardy, 2010].

In a situation of water stress, tolerant plants seek to expand their root system deeper [Gregory, 2008]. It has been shown by Bowen in 1985 that the extent of the root system is linked to the tree's capacity to perform in a situation of competition [Bowen, 1985]. A decrease in the relative humidity in the air increases the potential difference between leaves and atmosphere and therefore tends to increase transpiration. Stomatal closure arises during dry period because it helps preventing damages to the plant functionning [Tyree and Ewers, 1991].

The root depth and density play an important role in maintaining supply of water to the plant, especially if it is subject to drought. At the same time, features of the root system vary greatly with edaphic and climatic conditions: root growth is, for example, often hampered by obstacles such as the plow layer, but is also closely related to soil moisture. Moreover, these rooting features are also related to the genotype [Khaldoun et al., 1990].

The root development is heavily affected by the surrounding soil. In addition, possibly nutrients deficiency and other local parameters can influence the root growth, including a modification of the root architecture [Lobet et al., 2014].

2.3.3 Available water

All the water in the soil is not necessary available for plants. Water uptake in the soil is strongly dependant of the "soil water availability", defined as the potential range of a soil to hold back water, available for crops. This range is between the permanent wilting point (PWP) and the field capacity (FC), each corresponding to a certain potential and soil water content. The function between the soil water potential (ψ) and the soil water content (θ) is the retention curve [Romano and Santini, 2002].

The soil water retention function consists of three zones: the adsorption zone, the capillary zone and the air inlet zone (Figure 1). The adsorption zone is independent of the structure and conditioned by the role of clays and organic matter, because of the importance of their specific surface. The capillary zone, in turn, is strongly related to the structure and refers to the pore size distribution range. While the air entry zone corresponds to the porosity that will empty when the coarser pores release their water. The retention curve model developed by van Genuchten in 1980 is the most often encountered in the literature. This equation expresses the soil water content ($\theta(\psi)$) as a function of adjustment parameters $\alpha[L^{-1}]$ (which is related to the air entry point) and n [-] (which determine the slope of the curve) and ψ $[L]$ the soil matric potential :

$$\theta(\psi) = \theta_r + \frac{\theta_s - \theta_r}{[1 + (\alpha|\psi|)^n]^{1-1/n}}, \tag{12}$$

with θ_r the residual water content [Van Genuchten, 1980, Degré, 2017].

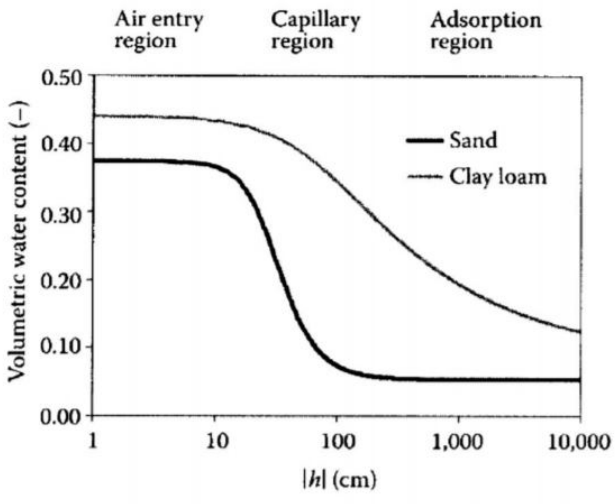

Figure 4: Theoretical retention function for a sandy-clay soil [Degré, 2017].

2.4 Link between isotopes and RWU

In the natural environment, water stable isotopes present a certain spatial heterogeneity in the different compartments of the soil-plant-atmosphere continuum [Barnes and Allison, 1988]. A mass conservation approach enables to find the proportion of each depth contributing to the RWU. This is done with the help of a multi sources mixing model. The sources refer to the depth to which water is extracted and analysed to obtain the corresponding δ. It is therefore possible to use the isotopes information to trace the water's origin. More information about the model are given in the subsection 3.7 of the materials and methods.

Studies on the isotopic analysis in hydrology are based on natural or artificial variations in δ^2H and δ^{18}O [Gat et al., 2001]. This latter variation can be done with the help of a label water (enriched in heavy or light isotopes) added in order to emphasize the tracer [Macaigne, 2011]. In this experiment, only natural variation are exploited.

2.4.1 Hypotheses

The current work is based on the assumption that the plant water uptake is not a fractionating process. It means that water does not undergo any change in its isotopic signature from the source in the soil and during the transport within the plant until the location where water is sampled in the crop (tillers). In this sense, the isotopic signal is transported in the xylem sap through the roots and is "isotopically" representative of the water mixture uptake at different depths of soil. This statement is on the basis of the use of water stable isotopes as tracers in the hydrological cycle, particularly in the RWU process [Macaigne, 2011].

While no isotopic fractionation occurs during the root water uptake, it can well happen during transpiration. Partitioning between evaporation and transpiration is by the way studied by several authors such as Rothfuss et al. [Rothfuss et al., 2010].

In the xylem water, an enrichment in heavy isotopes takes place because evaporation occurs at the leaves level. Therefore it is important for the xylem sap to be sampled in a zone where there is no enrichment due to evaporation [Kotz and Treichel Jr, 2006]. In 1993, Dawson and Ehleringer analysed δ^2H and $\delta^{18}O$ in the path water uptake of an Acer Negudo and confirmed this last hypothesis [Ehleringer and Dawson, 1992]. Concerning Hordeum vulgare, it has been "found to be relatively free of further fractionation" [Walker and Richardson, 1991].

A study carried out in 1987 by Dalton leads to the following conclusion: a small fraction of vapour water is also taken up by plants due to an enrichment of heavier

isotopes in the residual soil water. However, there is a consensus about the fact that only liquid water is uptaken by plants [Dalton, 1989].

Even if the isotopic analysis is a useful tool for the determination of RWU profile, it is important to mention that RWU varies in time and space. Therefore the study of RWU in link with its spatial and time variation could be restricted by the isotopes measurements, in terms of sampling frequency.

3 Materials and methods

3.1 Experimental site

3.1.1 Study site

The experiment took place in the agroforestery parcel of Gembloux Agro-Bio Tech in the Hesbaye region, Belgium. Landscapes of this region are dominated by agriculture with more than 80% of the land occupied by crops, meadows and more rarely orchards. The region owes its agricultural vocation to the thick mantle of loess deposited during the cold period of the Quaternary [Bernard Delcambre, 2002].

The study area is located to the east of Gembloux (Bordia Street). The exact location of the experiment (black cross in the figure 5) within the experimental field (blue frame in the figure 5), has the following geographical coordinate: 50°33'58"N 4°42'37"E. The following figure illustrates the location of the study plot (blue frame).

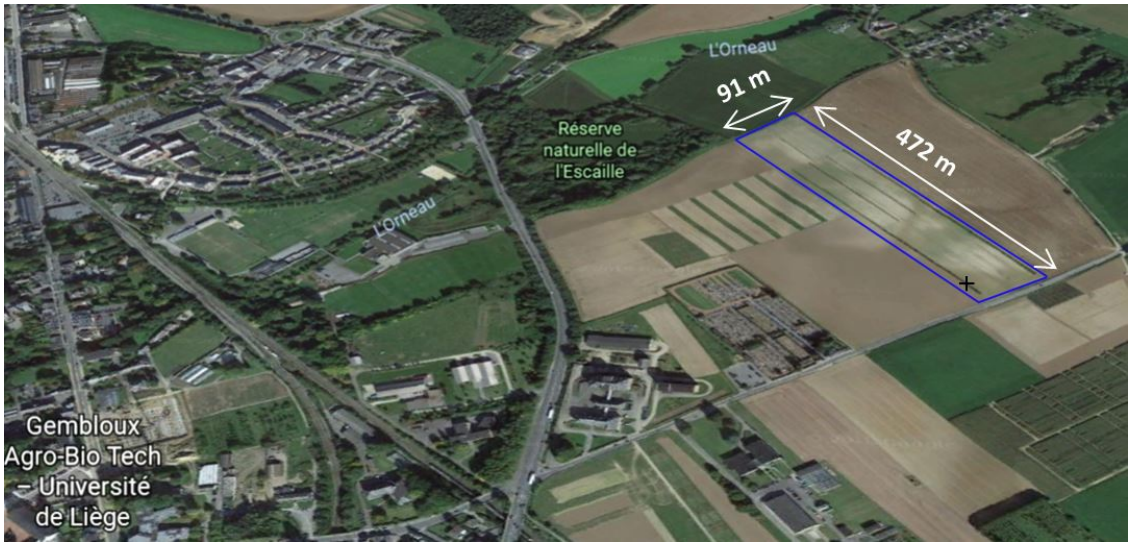

Figure 5: Localisation of the agroforestery field east of Gembloux Agro-Bio Tech. The field is represented by a blue frame and the exact location of the experiment by a black cross (Google Earth).

Figure 6: Picture of the site one week after the installation of the underground material needed for the experiment.

3.1.2 Soil profile

The soil of the experiment site (figure 7) has been categorised by the "Map of main soil types of Wallonia" as a silty soil with favourable natural drainage (code: Aba1). The "A" refers to soils having less than 30% of clay and less than 15% of sand. This type of soil is typical of the plateau of the "silty region" and have a great agronomic potential, considered as "a fertile heir of the periglacial period". In fact, the pedogenenesis of this type of soil (called "luvisol") is based on clay accumulation upon the profile. This phenomenon is linked to the nature of the parental material and is a preferential process that occurs with a loose sedimentary material. The geology of the region has two origins. The first one is the "Brusselian sands" that contains different sandy bodies and originates from the middle Eocene (Paleogene). The tickness of this layer varies from 20 to 40 meters. The second one is a loess deposit from Quaternary (Pleistocene) arised out of a silt windblown during periglacial period. The long weathering processes of these two parental material results in the formation of the actual soil [Hallet, 2015].

Before anthropogenic influences on soil, the profile could be described with three distinct horizons: Ap, E and Bt. However since agricultural activities took place, especially plough until 40 cm, it is henceforth not possible to distinguish the "Ap" and the "E" horizons, because the E horizon was mixed whitin the A horizon on more or less 40-45 cm with the previous ploughing activities. That is why two main

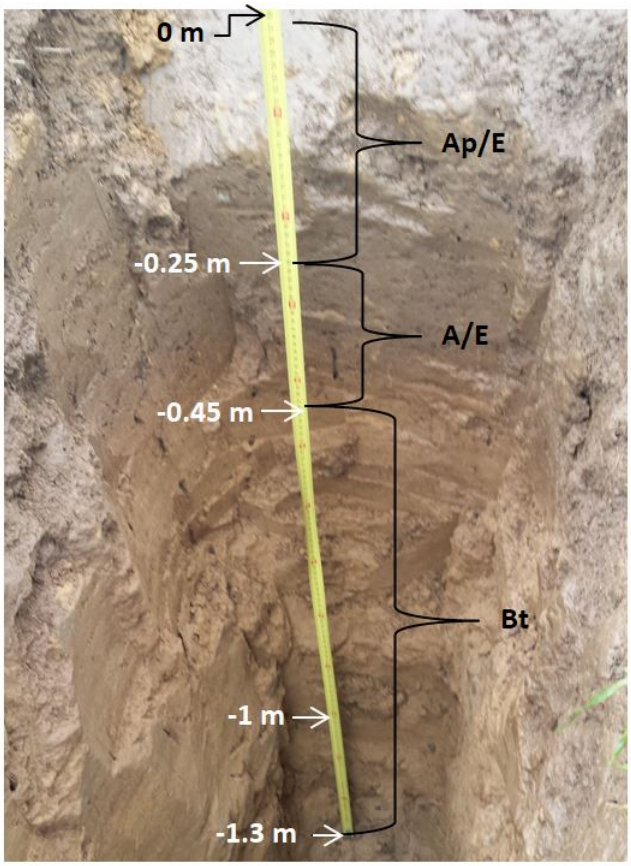

Figure 7: Picture of the soil profile with the three horizons represented.

horizons can be identified:

A(p)/E . The topsoil has been ploughed in the first 25 cm (characterised by the "p" for ploughing). But due to previous ploughing, Ap and E are mixed until approximetely 40-45 cm. This first horizon is a hemiorganic horizon, where the organic matter is incorporated and mixed with the mineral matter. This layer has a darker appearance than the lower horizon, because of its enrichment in organic matter. This horizon is depleted in iron and clay compared to the Bt horizon[Baize and Girard, 2008].

Bt. The "B" horizon means that it is enriched in particles or elements compared to others. In this case it is enriched in clay particles (the "t" in Bt refers to clay). The relatively compact layer can be an obstacle for root development for certain plant species. Nevertheless, it is neither stony nor affected by a water excess [Hallet, 2015].

The "C horizon" or the unaltered loess (parental material) generally reaches depths of more than 2 meters [Colinet, 2003].

Soil horizon	Depth	Description	Soil bulk density
Ap/E	0-25 cm	topsoil: ploughing surface	1.36 g cm^{-3}
A/E	25-45 cm	previous ploughing	1.55 g cm^{-3}
BT	45-130 and more cm	clay accumulation	1.54 g cm^{-3}

Table 2: The depth, a brief description and the soil bulk densities are given with respect to the soil horizon.

The apparent soil densities have been calculated for each soil horizon with undisturbed soil samples that keep their original structure. Standard procedure has been used (available on the intranet website of Gembloux Agro-Bio Tech). Three repetitions per horizon were performed and the mean bulk density is given in the last column of figure 2.

3.1.3 Crop and technical itinerary

Winter barley (*Hordeum vulgare L.*) was used in this experiment in its last development stages. Winter barley crop has a spread root system and can be extended until two meters deep.

Date	**Agricultural practices**
25/09/2017	plowing 20 to 25 cm deep
26/09/2017	sowing (variety Rafaela, 100 $kg.ha^{-1}$)
18/10/2017	weeding (Liberator, 0.6 $L.ha^{-1}$)
26/03/2018	nitrogen fertilization (nitrogen solution 39% (= liquid form), 67 $kg.N.ha^{-1}$)
10/04/2018	nitrogen fertilization (nitrogen solution 39%, 40 $kg.N.ha^{-1}$)
25/04/2018	nitrogen fertilization (ammonitrate 27% (= solid form), 65 $kg.N.ha^{-1}$)
02/05/2018	fungicidal treatment (Velogy Era 1$L.ha^{-1}$ and Bravo 0.5 $L.ha^{-1}$) regulator (Yatze 1$L.ha^{-1}$)

Table 3: Agricultural practices according to the date.

Rafaela is a variety that does not have to be inoculated with an insecticide: the sturgeon becomes resistant to the yellow dwarf virus infested by aphids. Even if the development of aphids is heterogeneous on the plot, yield losses affected by the yellow dwarf virus can be significant [Fabre et al., 2003].

3.1.4 Soil water retention curves

Hyprop® was used in order to identify hydraulic properties of soil samples with the help of the software tensioVIEW®. The soil water retention curves are gener-

ated with discrete measures and fitted with the van Genuchten Mualem equation. A rigorous monitoring was carried out, following the hyprop manual instructions. Therefore if more details about the hyprop use are needed, it is possible to refer to the hyprop manual [UMS, 2013].

Three soil samples have been analysed with Hyprop, each corresponding to a distinct soil horizon in the location of the field experiment (10, 40 and 100 cm deep).

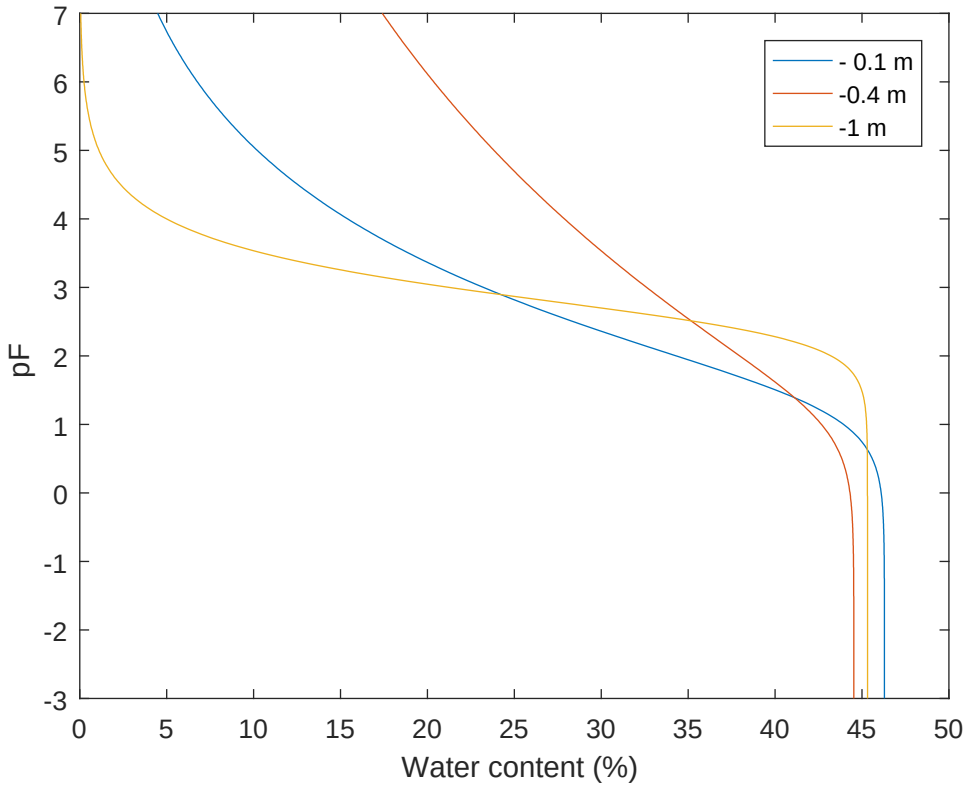

Figure 8: Retention curves obtained with Hyprop for three soil samples corresponding to the following depths: 10, 40 and 100 cm.

3.2 Soil water vapour extraction method

3.2.1 Application of the method

A recent promising soil water vapour extraction method using gas permeable tubing has been presented by Rothfuss et al. in 2013 an 2015 [Rothfuss et al., 2013, Gangi et al., 2015, Rothfuss et al., 2015]. The method was combined with infrared laser spectrometry online measurements. The Cavity ring-down laser spectrometer was a Picarro L1102-i and allows gases to be monitored online in a few seconds. This soil water vapour extraction method was tested and calibrated in laboratory with this continuous measurement system. In this MSc thesis's experiment, the determination of the soil liquid water isotopic composition was based on a cost-effective compromise, a variation of the method proposed by Rothfuss et al. The gas permeable tubing was first used in order to extract the soil vapour water. Then, instead of being combined with the laser spectrometer that monitors the δ of the water vapour online, the soil vapour stream runs into a trap immersed in dry CO_2 (dry ice, about minus 80°C) to be transformed into liquid water. Then the liquid condensed water samples are collected in inserts of 0.1 ml, each corresponding of the five soil depths. Water was analysed offline by a laser spectrometer (Picarro L2130-i of the Institute of Biogeosciences - Agrosphere, Forschungszentrum Jülich). The laser spectrometer measurement is based on the specific range of each molecule to absorb near-infrared.

This application of the method involves the extraction of water from the cold cryogenic traps. Indeed, at this step, water contained in the traps has condensed all around the edges of the glass (left picture of figure 9). It is necessary to collect all the water in order to have a representation of the isotopic composition and to avoid any fractionation process. To do so, two main methods are possible:

- Use the extraction line (of Jülich Center) that creates a water vacuum and extract 100% of the water from the trap (a picture of the extraction line is available in the appendix of this work).
- Create a temperature gradient with a hotgun (250°C) and a few dry ice. This process eases the vaporisation of the condensate water at the top of the trap and it allows to get all the water in the lower part of the trap at dry ice level (figure 9).

In this experiment, this second method was chosen for a practical question. In addition, we wanted to test if a more simple method was efficient. The proposed method does not use the hotgun but is only based on a the extraction of a bigger amount of water, that could potentially decrease the fractionation effect during the water extraction from the trap.

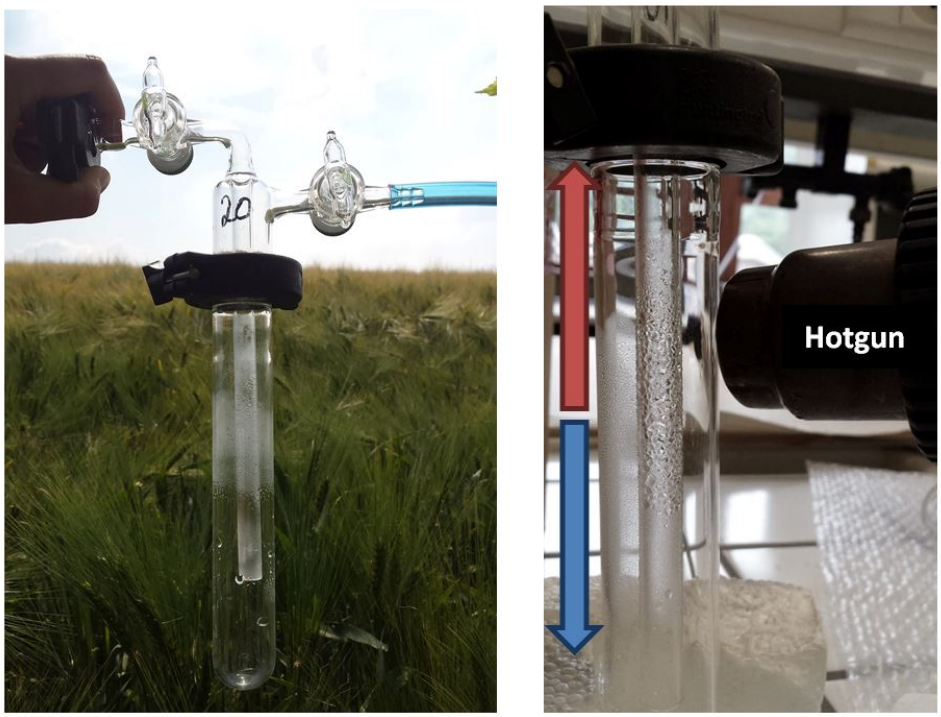

Figure 9: The left picture shows a soil sample water (extracted at 20 cm) in the trap. Condensation can be seen on the rim of the trap. The left picture shows the temperature gradient made with a hotgun (blowing air at 250°C) in the upper part and dry ice in the lower part.

Below are described the different steps of this variant field extraction method. Step 2 to 4 are shown in figure 10 while step 1 is explained in details in the next subsection.

1. Vapour water is extracted with gas-permeable tubes installed at different depths under the ground in the field.

2. Vapour water runs in the trap and is transformed into liquid water through the condensation process with the help of a dry ice immersion of the traps.

3. Liquid water is collected from the trap with a temperature gradient made in lab.

4. Isotopic analysis with a laser spectrometer in lab.

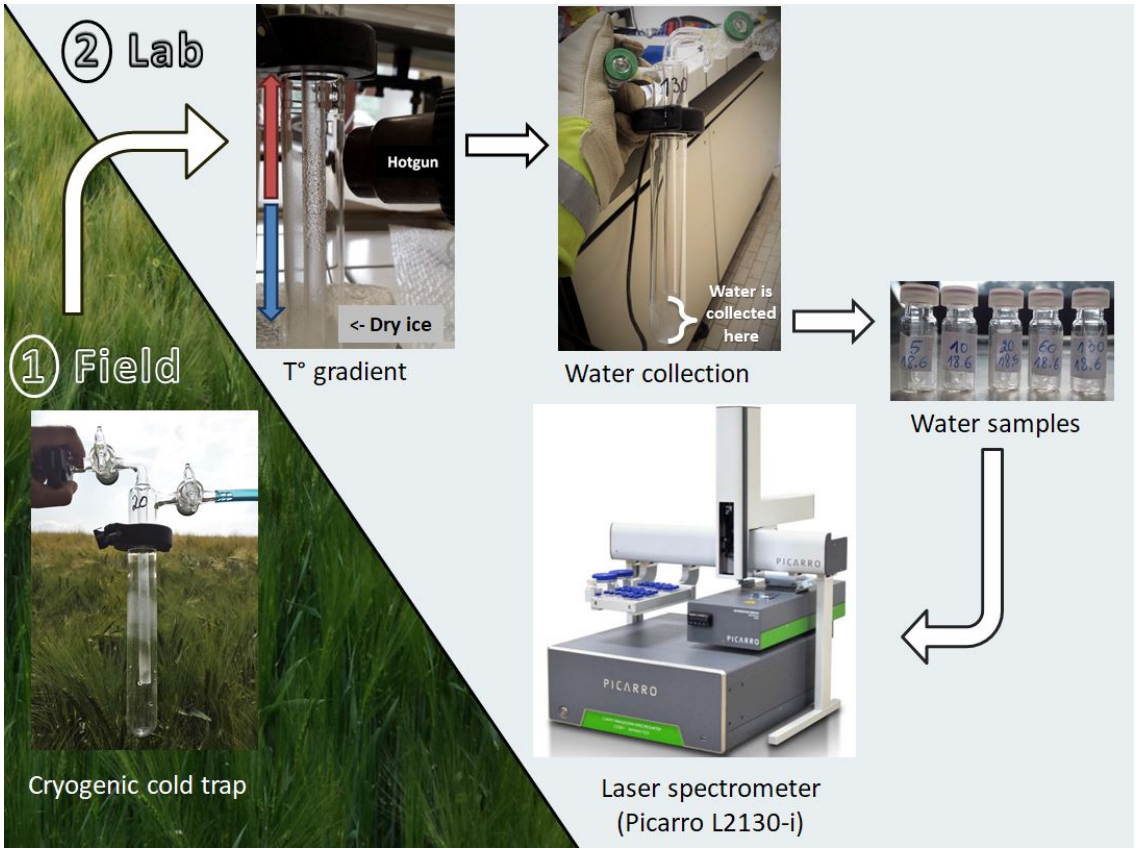

Figure 10: Different steps of the liquid soil water extraction from the trap: variant of the method presented by Rothfuss et al. The green part is the field part while the gray part represents the laboratory part.

3.2.2 Description and functioning of the method

The permeable tubing system can be deployed in the field. The present study is committed to test this method for the first time in real field conditions. Hence it renders possible to monitor entire soil profiles in the field, and, at a later stage to identify root water uptake depths from these profile isotopic measurements.

A set of 1 m length gas permeable polypropylene tubing ("Accurel® PP V8/2HF, Membrana GmbH, Germany; 0.155 cm wall thickness, 0.55 cm i.d., 0.86 cm o.d.") installed horizontally allows the vapour phase of the soil water to be extracted. The tubing micro-perforated (0.2 microns) plastic (polypropylene) walls lets the soil gas-phase enter its vicinity while giving him strong hydrophobic properties [Rothfuss et al., 2013]. Due to an applied pressure difference, water vapour is able to come inside the tube. This variation of pressure is obtained by running dry air through the tubes, connected to a dry air bottle (AirLiquid®, alphagaz 1 air, composed of N_2 at 20% and of O_2 at 80%) and linked with 6 mm polyethylene composite

tubing Synflex®. Every tube are linked with each others with Swagelok® fittings.

A the soil pore scale, soil water is in thermodynamic equilibrium between its vapour and liquid phases. In this work, the underlying assumption that thermodynamic equilibration prevails during sampling is made. Therefore it is necessary to use temperature dependent calibration equations in order to obtain the $\delta^2 H_{liq}$ and $\delta^{18} O_{liq}$ from the measured $\delta^2 H_{vap}$ and $\delta^{18} O_{vap}$ at given temperature. These equations slightly differ from those of Majoube et al. (1971) as the removal of water vapour is different and the properties of the permeable tubing have an impact on the (mostly hydrogen) isotopic composition of soil water vapour. The equations read:

$$\delta^2 H_{liq} = 1.235 \cdot \delta^2 H_{vap} - 1.657 \cdot t + 129.702, \tag{13}$$

$$\delta^{18} O_{liq} = 1.131 \cdot \delta^{18} O_{vap} - 0.095 \cdot t + 14.998. \tag{14}$$

with t, the temperature in °C, δ_{liq} refers to liquid and δ_{vap} to the vapour form of the water isotopic composition [$‰_0$].

A constant flow of synthetic dry air is maintained. This controlled pressure allows a steady flow of dry synthetic air inside the permeable tubes. The aim is not to influence the isotopic signature of stable H and O. Hence the air is pushed in the tube and no vacuum is applied. Because a vapour pressure gradient is applied, a circulation occurs. At this level it is important not to apply a too high pressure in order not to disturb the surrounding soil to the point of disrupting the isotopic thermodynamic equilibrium established between the two phases in the soil. According to Rothfuss, a flow of 100 $ml \cdot min^{-1}$ per tubing is sufficient [Rothfuss et al., 2015]. A flow regulator (Agilent® Technologies Flowmeter Reverse Flow, ADM 3000) is used to control the incoming flow. After 30 minutes of flushing the system, a constant water vapour mixing ratio is reached and the vapour water sampling can begin. This time lapse was observed during a laboratory work of Rothfuss et al. (2013). During the sampling, the cryogenic traps are partly immersed in dry ice to trap all the water vapour. The dry ice temperature is about minus 80°C. The system "trap and dry ice" is installed in a Dewar (KGW-Isotherm® cylindrical Dewar Flask) itself contained in an insulating box (fridge box). The aim is to avoid heat losses and therefore, dry ice loss. The box was further insulated with insulated sheets (Armacell®, Armaflex, USA) in order to avoid dry ice sublimation. The extraction takes about 2 hours depending on temperature conditions.

The dry ice is produced in the laboratory prior the field sampling with a CO_2 bottle (AirLiquid®, CO_2). The picture on figure 11 represents its making process. Solid CO_2 is directed recovered in a SnowPack (Bürkle® GmbH, Germany). A thick

polystyrene box is then used to store and isolate the dry ice, but also to carry it to the experimental site.

Figure 11: Design and picture of the dry ice making in order to cool the soil water vapour and force condensation of water vapour extracted.

3.2.3 Field experimental setup

On the one hand, figure 12 represents the design of the soil water extraction device in the field (set of gas permeable tubing). On the other hand, figure 13 shows a schematic representation of the setup in the field with the Synflex® tubes only for one repetition (instead of three) and with one Dewar represented (instead of five). In addition, the position of the 5TM® soil moisture and temperature probes is represented by the red cross in this figure.

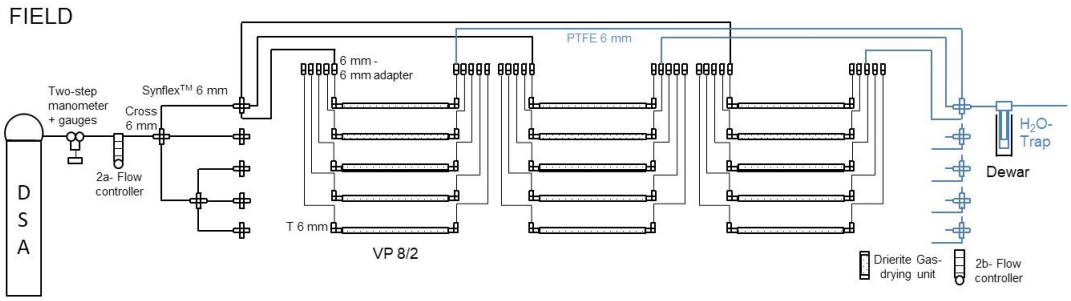

Figure 12: Design of the soil water extraction device in the field.

Three repetitions of the extraction system at five depths are performed. The aim is to harvest enough water, but also to increase the spatial representativeness of the isotopes profile in the field. In order to have a representation of the isotopic

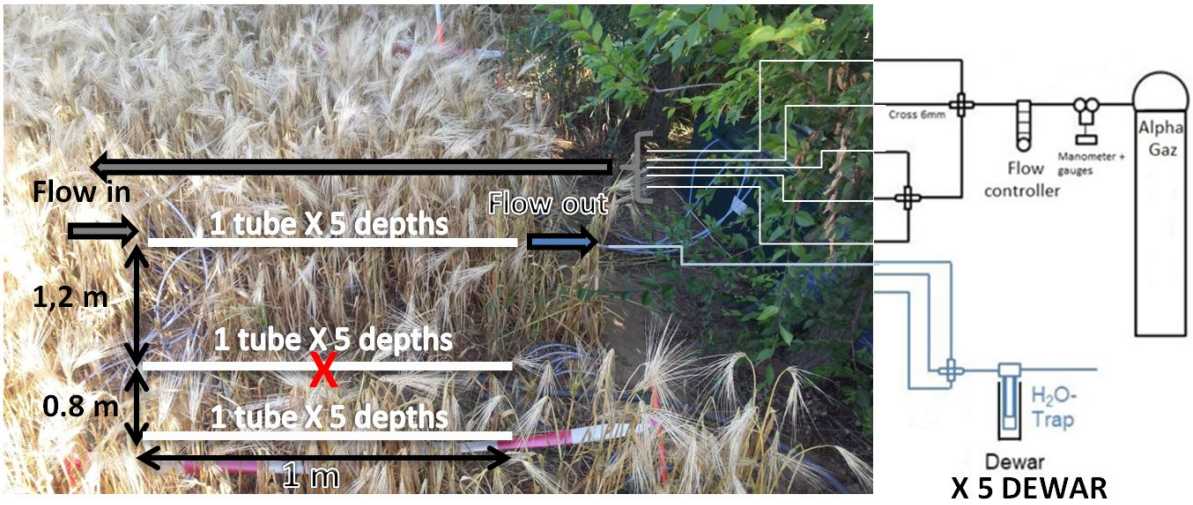

Figure 13: Design of the soil water extraction device in the field. This schematic representation shows the device for one tube. The red cross indicates the position of the 5TM soil moisture and temperature probes.

variability within the soil, it is necessary to obtain enough data in the upper part of the soil. Indeed, the isotopic variability is bigger near the soil surface. Therefore water vapour will be extracted for this experiment at 5, 10, 20, 60 and 130 cm.

3.3 Sampling of the xylem water

During the time period the soil water vapour was being extracted, plant samples were taken from the field. The extracted plant parts lie at the base of the plant to the first internode of the tillar. The sampling zone was determined not too far from the soil isotopic profile measurement so that the isotopic composition of the xylem sap was representative of the RWU related to the soil profile. It was located 5 meters right and left in the extension of this isotopic profile, which is visible on figure 14. The idea was to leave all the plants in the zone where the set of fifteen gas-permeable tubes were installed, in order not to disturb this zone, already impaired by the construction of the two digs in April. The aim was also to maintain the influence of plants on the soil isotopic profile. A box full of about fifty tillers samples were sent each time. From these fifty tillers samples, only three were taken for the extraction because an enough amount of water was obtained for the use of the laser spectrometer. The line extraction was used to extract water molecules from the plant. Plant water samples contained a too high level organic matter. They had to be treated before an isotopic measurement with the laser spectrometer could take place.

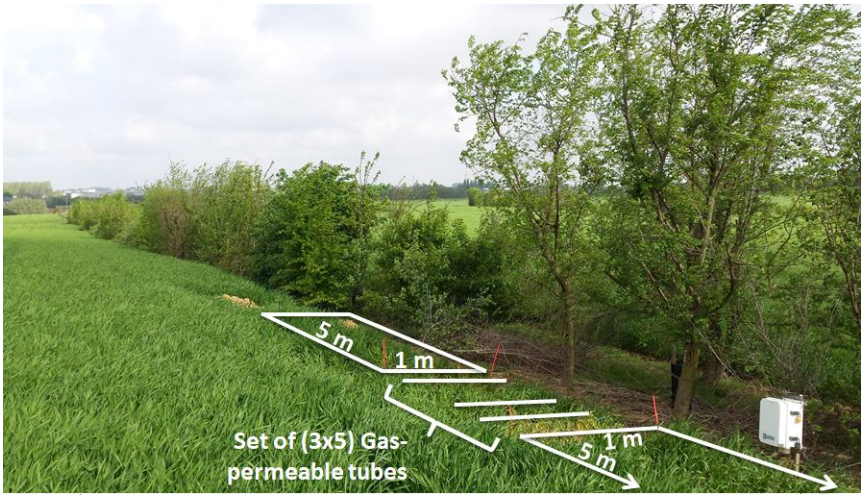

Figure 14: Schematic design of the plant's sampling zone, located in the white frames.

3.4 Measure timing

From May to June, eight experiments took place in the framework of this MSc thesis. Each time, a particular attention was given to the weather forecast, in order to avoid a raining event during the sampling, that could highly affect the isotopic composition data.

3.5 Soil moisture and temperature monitoring

Next to the water vapour extraction tubes, we also installed soil moisture and temperature probes (Meter Group®, 5TM) at five depths (table 4) linked to a data logger (Meter Group®, Em50). A calibration equation linking the dielectric permittivity (raw output data of the sensor) to the water content has been developed by Topp et al. for mineral soils [Greaves et al., 1996]. The probes have been calibrated for temperature and soil volumetric water content in order to have their fitting response in the typical soil of the experiment. This has been done following a standard procedure (accessible on the intranet website of Gembloux Agro-Bio Tech). Calibration equations (fitted with the software CurveExpert Basic®) are given in the appendix of this work. In addition, a moving average has been employed for sensors at -0.075 m and -0.2 m because sensors are sensitive to temperature changes at this depth. The accuracy of a 5TM probe is about $\pm$ 0.03 v/v (for ξ_a) and about $\pm$ 1°C (for temperature) [Devices, 2017].

5TM sensor	sensor depth (m)	soil horizon
1	-0.075	Ap/E
2	-0.2	Ap/E
3	-0.6	Bt
4	-0.95	Bt
5	-1.3	Bt

Table 4: 5TM sensor depths and matching horizon.

3.6 Root Length Density measurements

We performed destructive Root Length Density (RLD) measurements at the end of the experiment. The RLD is defined as the total length of the roots in a soil volume [$cm.cm^{-3}$].

3.6.1 Soil sampling

Soil cores were sampled manually with a soil auger of a known volume at three different locations (corresponding to three repetitions) in the plant's sampling zone of the figure 14. The aim was to have a representativeness of the root systems of plants that were used for xylem sap water analysis during the experiment. The left picture of the figure 15 shows the sampling with the auger.

Figure 15: The left picture shows the soil cores that are sampled manually with an auger in the field. The right picture shows the device to separate and wash the roots from the soil samples.

3.6.2 Roots washing

A device shown in the figure 15 was used in order to separate the roots and the ground from soil cores. One advantage of the automatic washing is the standardisation of the process [Smit et al., 2013]. A water flow swirls and lets the dirty water leave the seal until the water inside is clean. Remaining elements (including roots,

crop residues and stones) are retained through two overlapped sieves in the middle of the seal. The remaining elements were stored within two thin screens in an oven at 60°C during a week. Dried roots were then easily separated from the stones.

3.6.3 Roots scan

The roots were manually spread out in the petri dishes of 12.5 cm square shape. In order to ease the sprawl and to remove any bacteria contamination, roots are beforehand stored in a solution of 60% of ethanol and 40% of water. Roots samples sat in that solution in a cold chamber before the scan. The roots are spread with the help of distilled water that was added in the petri dishes. A thin plastic layer was put on the top of the roots, after removing the water with a syringe.

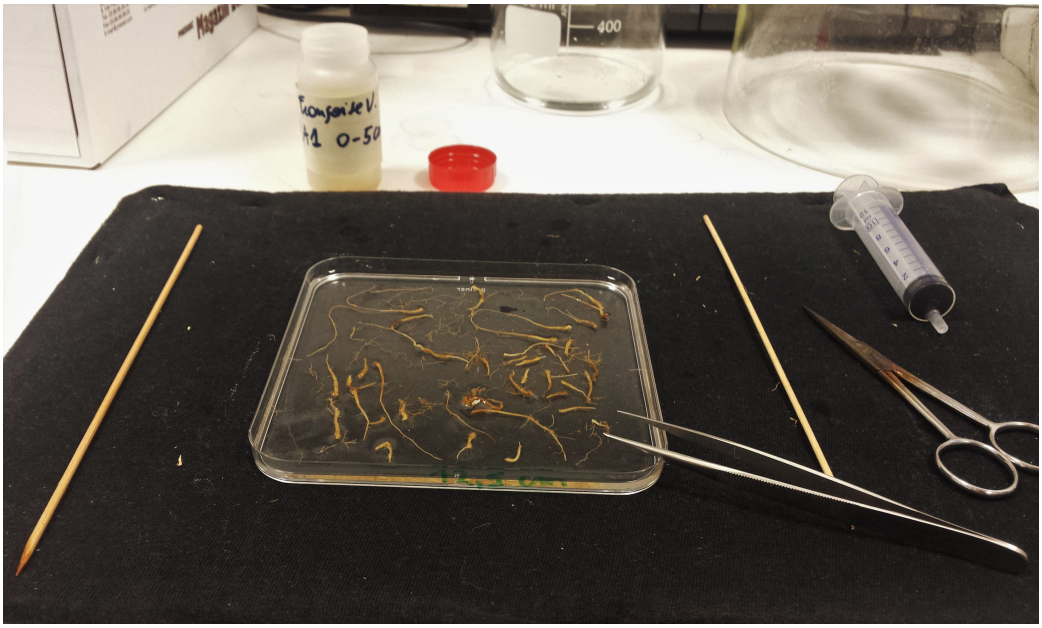

Figure 16: Selection and extend of the roots before the scan in a water solution.

The resolution of 400 dpi or "dot per inch" (one inch is equal to 2.54cm) was chosen because the image analysis does not take into account the tiny hair in the calculation of the root length with such a low resolution. A 1200 dpi resolution is for example too high to avoid this problem. One root was used as a standard. It was first drawn on a graph paper and measured by hand, to be sure that the calculated root length was equal to the measured one.

3.6.4 Image analysis

Roots images were analysed via the software ImageJ® . An example of an analysed image is given in the figure 17. Below are the steps that were followed in Image-J in order to have an automatic calculation of the lengths.

- Set the scale, based on the 400 dpi resolution, where 400 pixels are represented by 2.54 cm.
- Remove the edges of the box (and eventually air bubbles or any remaining crop residues) with the paintbrush tool or by cropping the image.
- Transform the image into a 8-bit image, black and white.
- Adjust a treshold in order to have a binary image.
- Transform each root into segment with the "skeletonise" tool.
- Analyse particles from 0.002 cm^2 to ∞ area. It allows to discard particles inferior to 0.002 cm^2 that are not roots. The perimeter of each particle is automatically calculated. It is necessary to sum all of them and divide them by two in order to have the total roots length.

Figure 17: Example of transformed and analysed image with ImageJ; the left picture is a scan of the roots and the right picture is the same image after treatments.

3.7 Determination of RWU profiles with statistical modeling

Most of the studies concerning isotopic analysis of water in the natural environment have been carried out under statistical analysis [Rothfuss and Javaux, 2017]. According to Rothfuss and Javaux (2017), there are four ways to obtain the RWU profile based on the isotopic signature. These are the "direct inference", the "multi-source mixing models, the "two-end member linear mixing model", and the "physically based numerical models" [Rothfuss and Javaux, 2017]. All methods involve an inverse model through optimization of the input data.

The multi-sources mixing model is the one used in this study (also used in 32% of the studies of water stable isotopes to retrieve RWU). The mixing model is typically used when plants extract water in at least three layers of the soil (i.e. there are at least three sources of water accounted for) [Phillips et al., 2014]. "Stable isotope mixing models are a potentially powerful tool for ecologists and can be used to quantify relationships that would otherwise be difficult or impossible to describe" [Moore and Semmens, 2008].

3.7.1 Model input

The inputs of the model are the information concerning both the "sources" and the "consumer". On the one hand, sources are the isotopic compositions of soil water for each depth (δ_s). On the other hand, the consumer is the isotopic composition of the plant xylem sap (δ_{ti}). The prefix "ti" refers to the "tiller" of the plant, where the water is extracted for the spectrometer analysis.

3.7.2 Model run

Calculations are based on a mass balanced mixing model. If we consider that there are N layers of soil, the xylem sap isotopic composition of the tillers (δ_{ti}) is equal to:

$$\delta_{Ti} = \sum_{j=1}^{N} X_j.\delta_{s,j}. \tag{15}$$

with X_j, the respective contribution of every water source corresponding to a specific soil layer (j) to the plant water uptake. The isotopic composition of soil water to the depth j is $\delta_{s,j}$. We also know that the total of each proportion is equal to 1:

$$\sum_{j=1}^{N} X_j = 1. \tag{16}$$

In this case, the number of solutions is unlimited because the number of water sources, or soil layers (5) is bigger than the number of mixing equations more one

(3). But some solutions are more likely to occur. All suitable solutions are found via iterative algorithms (Markov Chain Monte Carlo). This algorithm is used to fit the model to the data. In R, the package "SIAR" allows the use of the function "siarmcmcdirichletv4". This last function was used with a number of 2 000 000 iterations, 50 000 burnin (the number of iterations rejected) and 15 thinning.

3.7.3 Model outputs

After the run of the function, an R object filled of 10 000 lines is created, where each line of this object represents the share of each depth in the plant water extraction. The sum of each depth proportion (or a line) equals 1. The number of the total lines is calculated regarding the number of iterations, burnin and thinning:

$$\text{Lines number} = \frac{2\ 000\ 000 - 50\ 000}{15} = 10\ 000. \tag{17}$$

At this level, it it possible to know the number of times each proportion occurs for every depth. Subsequently, a certain number of classes are defined in order to smooth the density curve. In this case, the number of classes was 400. Therefore we can draw a density curve for each depth. The most frequent value (MFV) can be detected as the value to which the occurrence is maximum: its occurrence probability is the highest. These MFV are the final output, in the sense they provide information on where water is taken from the soil by the plant.

The uncertainty of δ_{ti} is taken into account by adding two data to which the standard deviation is subtracted or added. The model ran with a standard deviation for δ_{ti} equals to $\pm$ 1 or 2 ‰ (respectively for O and H) and $\pm$ 0.1 or 0.2 ‰ (respectively for O or H). The uncertainty of $\delta_{s,j}$ are also taken into account because they are comprised in the input data matrix.

Philips et al. reviewed the "best practices" for the isotope mixing models users [Phillips et al., 2014]. It is said that recognition of the limitations and the assumptions of the method is essential. A wrong use of the mixing models by the user is possible such as a negligence of uncertainties [Phillips and Gregg, 2001]. The integration of all sources uncertainties in mixing models is challenging and essential in a context where isotopes are more and more used [Moore and Semmens, 2008].

The more the isotopic compositions of the sources are contrasted, the more the mixing model is appropriate for the study of the root water uptake distribution for example. Therefore the number of sources can be low to keep the discriminatory power of the model [Phillips et al., 2014].

3.7.4 Model priors

The bayesian approach is convenient for several reasons. One of them is the possibility to include "extra" data such as the root length density and the soil moisture content. These extra data are used as a prior information in the model. The model may run using these priors: when initial proportions are specified before the iterations. In this study, two cases will be investigated. On the one hand, no prior data is inserted in the model. By default, the prior model is based on a Dirichlet prior distribution. The Dirichlet distribution is generalisation of a statistical distribution, called "beta distribution". In this "no prior" configuration, the model considers that each depth has the same contribution to the RWU. On the other hand, prior information is given to the model in order to constrain it. In our case, prior information is based on the RLD and the Soil Water Content (SWC) that were measured in situ. A vector of prior information, (18), will be calculated based on equation that was previously used in a paper of Mahindawansha [Mahindawansha et al., 2018]. The priors are normally distributed around p_j, a relative variable that is defined as

$$p_j = \frac{RLD_j \cdot SWC_j}{\sum_{k=1}^{5} RLD_k \cdot SWC_k}, \tag{18}$$

where SWC is the Soil Water Content in [%], RLD the Root Length Density in [cm cm^{-3}], j is fixed for one source (or depth) and k varies from the first to the fifth depth. In other words, the probability of one source that has a high RLD and SWC is higher to contribute to the RWU. It is important to know that in Bayesian statistical methods, prior information highly influences the final results. That is why the integration of additional information (RLD and SWC) to the model could give a more plausible response. One objective of the present study was to demonstrate this.

The measure of the standard deviation related to the p_j value were approximated by the means of first order Taylor approximation. partial derivatives are then:

$$\sigma^2_{p_j} = \sum_{k=1}^{5} \left[\left(\frac{\partial p_j}{\partial R_k} \right)^2 \cdot \sigma^2_{R_k} + \left(\frac{\partial p_j}{\partial S_k} \right)^2 \cdot \sigma^2_{S_k} \right], \tag{19}$$

with S, the abbreviation for the SWC, and R, the abbreviation for RLD. More details about the calculation are available in the appendix of this work.

4 Results

In this section results are presented regarding the objectives of the work. In total, eight measurements took place in the course of this MSc from the 17^{th} of May to the 20^{th} of June 2018. The soil water vapour has been extracted with the method above mentioned as well as xylem sap water in parallel. First of all, a time schedule of the experiment is given, as well as the respective development stage of winter barley.

Table 5 presents each soil and xylem water extraction in time. It also indicates the main cereal development stages with respect to the day of the experiment. The main cereal development stages and the stage number are based on the BBCH scale for cereals and field observations. The final cereal harvest happened the 2^{th} of July. This year, the development of winter barley was ahead of time compared to previous years, because the season was relatively hot and dry.

Within the next sections, the format "Date [number]" will be used to refer to the experimentation day in order to ease the reading of the results.

Date	Day	Main cereal development stage	Stage number	Extraction time
Date 1	17/05	Grain development	71	150 min
Date 2	23/05	Grain development	71	150 min
Date 3	29/05	Grain development	73	90 min
Date 4	04/06	Grain development	73	120 min
Date 5	13/06	Grain ripening	83	180 min
Date 6	15/06	Grain ripening	85	120 min
Date 7	18/06	Grain ripening	87	80 min
Date 8	20/06	Grain ripening	89	180 min

Table 5: The dates of the experiments, their day in the year, the main cereal development stage, the stage number referred by the BBCH scale, as well as the extraction time.

4.1 Soil water vapour extraction: quantitative outcomes

In this part of the work we test the following hypotheses: i.1) Enough water vapour can be harvested under field conditions to measure the isotopic concentrations. i.2) Field extraction is sufficiently rigorous to avoid problems of contamination during the extraction of water vapour.

The figure 18 shows the total volume of soil water sampled for each depth (five depths) for the last four experimentation dates (Date 5, Date 6, Date 7 and Date 8). The indicated flow gradient is the incoming flow of dry air that comes in each cold trap, measured with the flowmeter. The graph shows a positive correlation between the incoming flow and the water volume harvested. In addition, the extraction time is also positively correlated to the final volume harvested. The extraction times are referred to in table 5.

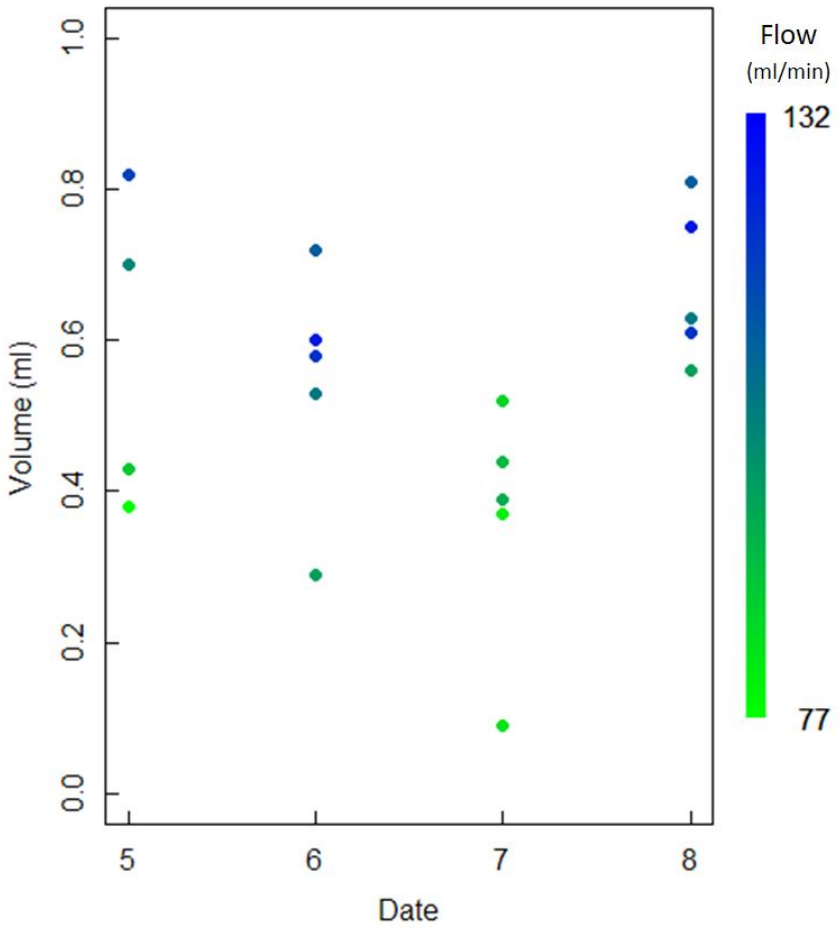

Figure 18: Soil water volume harvested at each depth for the last four dates of experiment (Date 5, Date 6, Date 7 and Date 8). The color gradient indicates the measured incoming dry air flow before each cold trap.

Globally, the graph clearly shows that for each depth and date, a sufficient quantity of water was collected. At least enough water was collected for the purpose of the analysis with a laser spectrometer, which had to be minimum 0.1 ml. However, we can see on the graph that for the Date 7, one soil water sample was too small (less than 0.1 ml) for the use of the laser spectrometer. The water isotopic composition of water collected at this date and depth (-0.1 m) could not be measured. Therefore, in the next sections, only four depths will be considered for the Date 7. This problem was due to the fact that the air inlet hole has been obstructed by the vacuum grease, used to insure an ointment of the trap. The incoming air was then blocked and not enough water was harvested that time. Concerning the Date 5, the volume harvested at -0.05 m and -1.3 m was the same amount, that is why we only see four points on the graph for this time.

As expected, the longer the extraction time, the larger the water volume harvested, and the graph clearly shows this effect. The two larger mean volume collected are for Date 5 and 8, then Date 6 and 7, with the respective extraction times of 180, 180, 120 and 80 min (table 5).

4.2 Environmental parameters

Some environmental parameters will be given in order to contextualise the field experiment. Figure 19 shows the soil and the air temperature conditions and its evolution through time. Soil temperature data, measured with 5TM probes, are presented after calibration. Air temperature has been provided by the local meteorological station of Ernage (IRM). Globally, soil temperature decreases with depth and tends to stabilise at a certain depth. On the contrary, the daily cycle evolution of temperature is detectable in surface. It is also remarkable that mean soil temperature tends to increase through the season. The variation amplitude of temperature is higher in the air than in the soil. We can also see that soil temperature changes with a little time lag compared to air temperature. This is because the soil needs more time to adjust its temperature compared to the atmosphere.

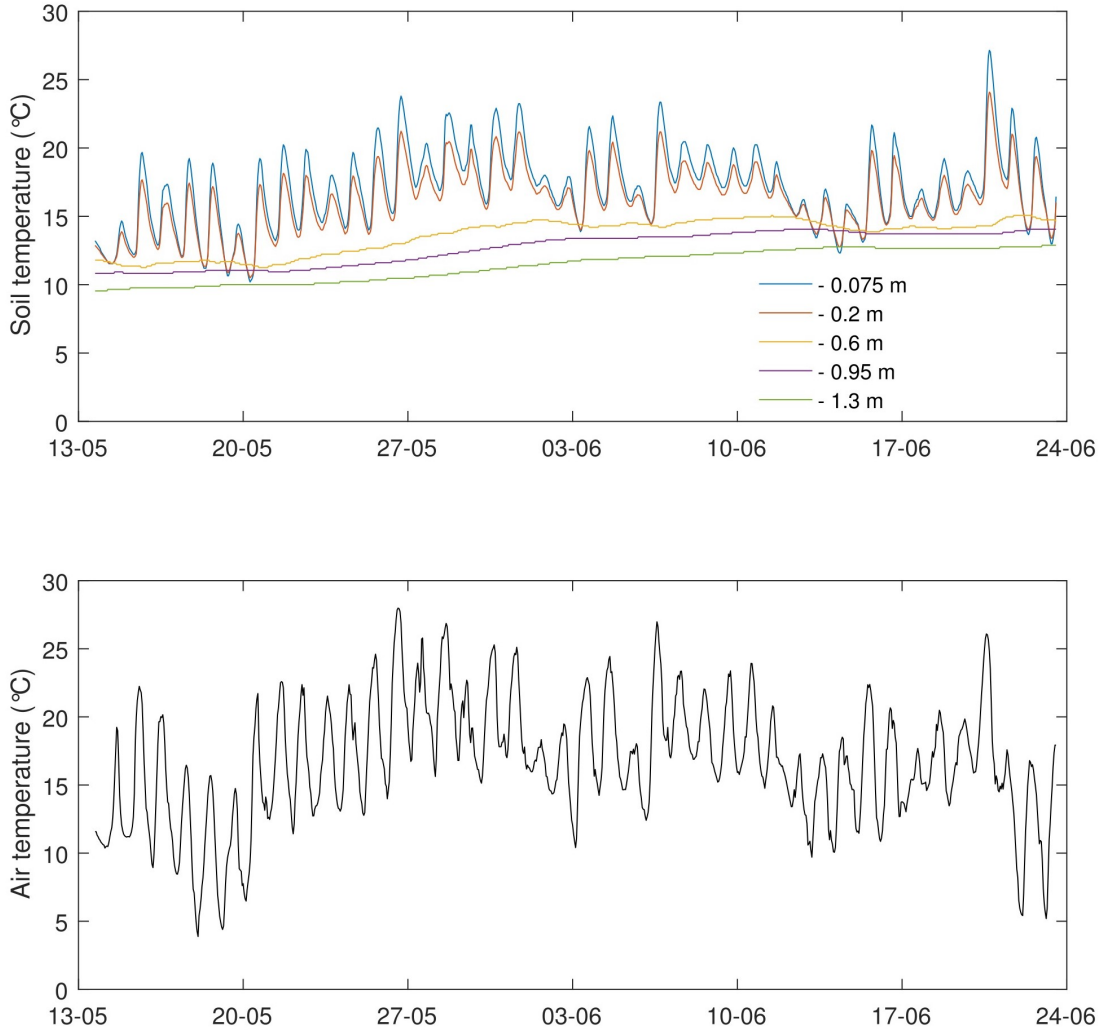

Figure 19: Soil and air temperature conditions and their evolution through time.

Natural parameters, such as precipitations (in mm) and air relative humidity (in %) and their evolution with time are presented in the figure 20. The red diamonds localise the eight experiments in time as well as their value of precipitation or relative humidity during the soil water vapour extraction. We can notice that only a few rain events happened at the end of the springtime and rain events are not regular in time. It was always raining before the extraction but no heavy rains was recorded, except the one of 25^{th} May, when the precipitation reached 7 mm in one hour. On the other hand, we can see that the air relative humidity varies daily. And the relative humidity conditions varies according to the extraction time.

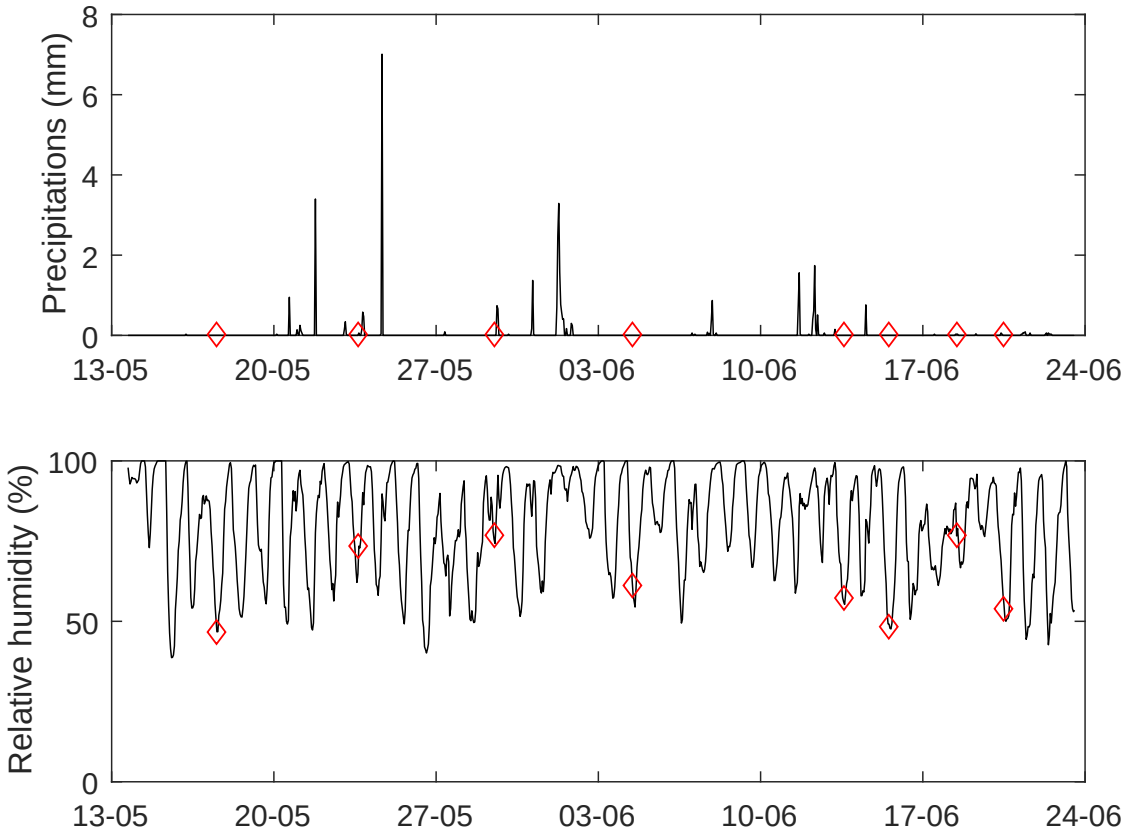

Figure 20: Evolution of precipitations (in mm) and relative humidity (in %) through time. The red diamonds localise the eight experiments in time.

4.3 Prior information in the model: RLD and SWC

4.3.1 Evolution of volumetric soil water content with time and depth

First of all it is important to figure out how data will influence the prior information. As a reminder, prior data is a vector constructed for each time and depth based on the RLD and the SWC. The aim of prior data is to shape the RWU profile. The figure 21 shows the evolution of the volumetric water content for each soil depth with respect to time, from the beginning of the experiment to the end. These data are given after calibration of the sensors. The volumetric water content varies most from day to day near the surface compared to other depths. It is at -0.075 m, that the soil is the dryest. Even if the water content at -0.2 m slightly follows the trend of the one at -0.075 m, the soil is drying through the season. The volumetric water content remains relatively constant in deeper depths (-0.6, -0.95 and -1.3 m) across time. Surprisingly, the water content at -0.6 m is almost twice bigger as compared to the one in -0.075 m.

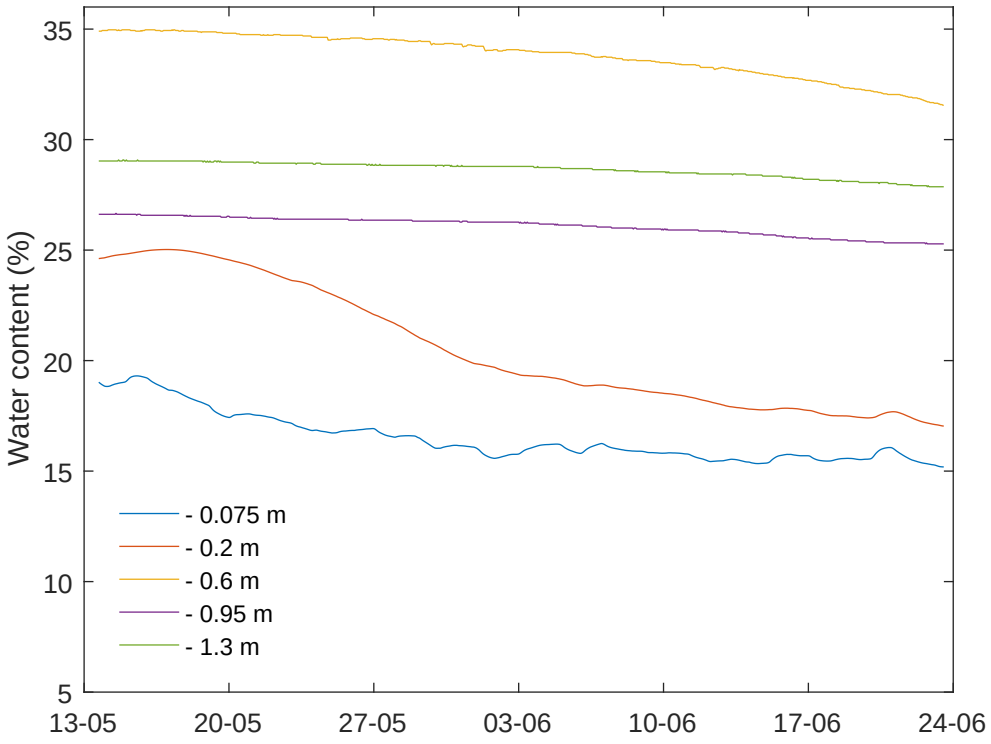

Figure 21: Soil volumetric water content measured by the 5TM probes and its spatial and time evolution.

4.3.2 Evolution of the Root Length Density with depth

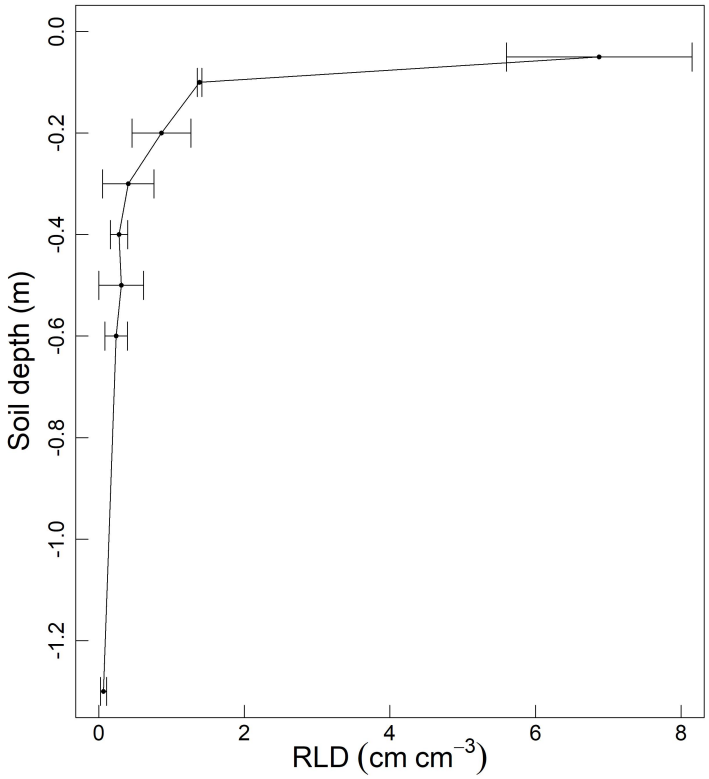

Figure 22: Variation of the RLD in (cm cm^{-3}) through depth with the respective standard deviation.

The evolution of the mean RLD through depth is shown on the figure 22. The standard deviation is represented by the horizontal bars for each measured point. First of all, the mean RLD tends to decrease exponentially with depth. Roots are mainly extended in the 30 first centimetres in the soil. Only a few roots were found at 0.6 and 1,3 meter deep. Secondly, it is interesting to point out that the standard deviation is quite different for each depth. For the first horizon, the standard deviation is the greatest, because the number of tillers of each plant varies a lot for cereals. Moreover, there were only three repetitions for each depth. As a reminder, roots were collected at the end of the experiment so this representation of the RLD is fixed in time and only available for the last stage of the winter barley. We therefore assume in this work that the RLD is constant during the last developing month of barley.

4.4 Variation of $\delta^2 H$ and δ^{18}O, temperature, soil moisture content and potential with depth

The figure 23 indicates the soil temperature, the volumetric water content, the plant and soil water isotopic composition through depth for each time step. Linear interpolations are done between each measured point.

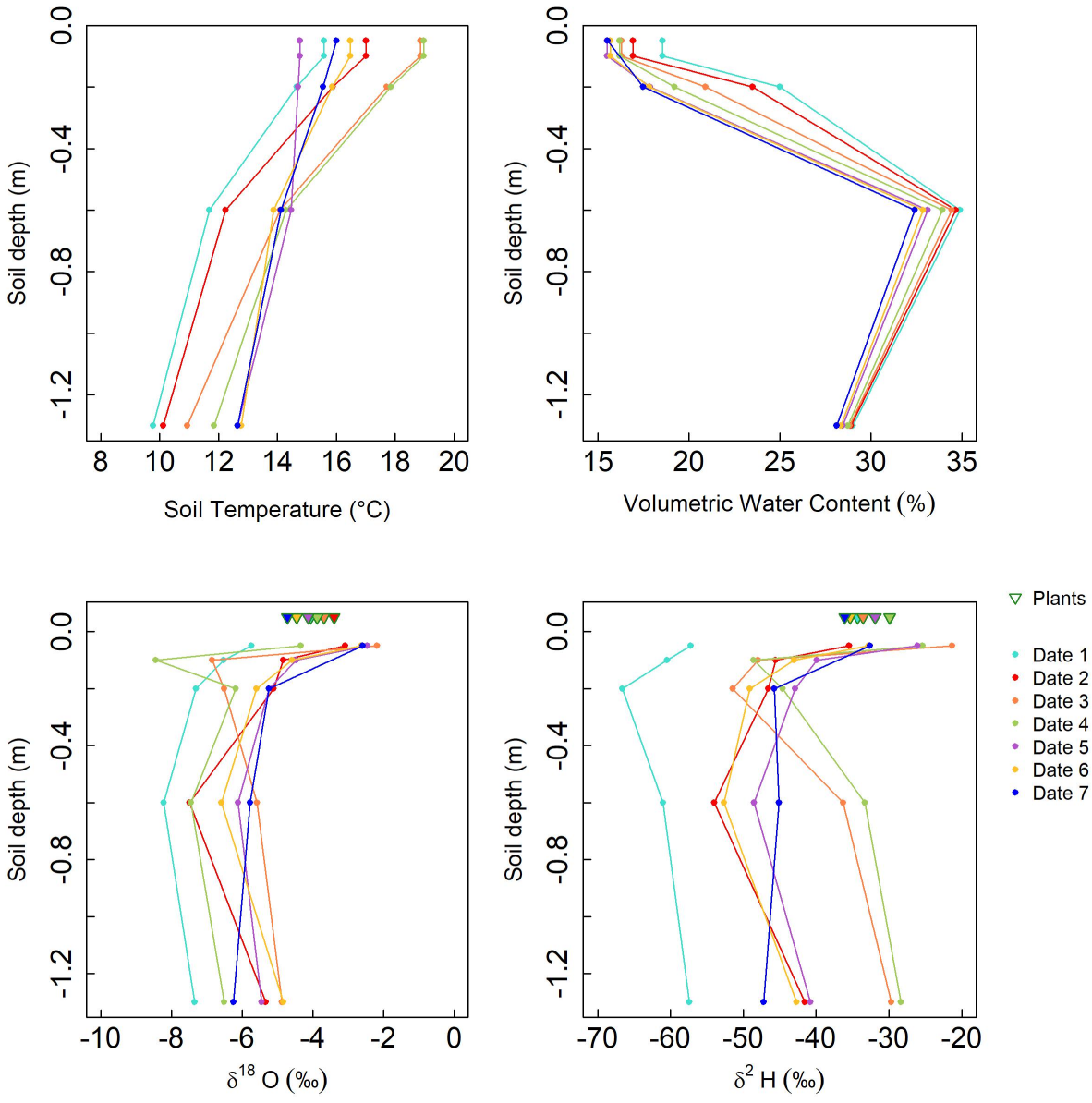

Figure 23: Evolution of soil temperature, volumetric water content, plant and soil water isotopic composition through depth for each time step.

First of all, the δ_s and δ_{ti} of the Date 8 were not inserted in this work for a logistical reason. As a result, only Date 1 to 7 are analysed.

Globally, temperature tends to be higher near the soil surface. For the three last Dates (Date 5, Date 6 and Date 7), temperature decreases a little from 0 to 0.6 m deep. The variation of volumetric water content is low from May to June.

An important isotope gradient occurs near the soil surface, while more deeper, this gradient tends to decrease. We can notice that values of δ^{18}O and δ^{2}H through depth are shifted from one date to another one.

Xylem sap water isotopic compositions (δ_{ti}) are represented as triangles with green outlines at the "soil surface" on the graph. They all are located within the soil water isotopic frame of the corresponding date, except for the Date 1 and Date 4. This confirms the fact that δ^{18}O and $\delta^{2}H$ of Date 1 and 4 are too isotopically depleted. It is important that the δ_{ti} are aligned with δ_s for the significance of the data.

The evolution of δ_{ti} through the season is very clear for O. Indeed, there is a clear shift of these data to the left through time. Before running the model, one could expect to have a deeper RWU patterns in soil from May to June. Concerning H, the same trend occurs, except for Date 3 and Date 4. Date 2 and Date 4 have almost exactly the same $\delta^{2}H$ so that we cannot differentiate them on the graph. As well as Date 1 and Date 5 for $\delta^{18}O$.

Precipitation patterns influence the isotopic profiles. The "Online Isotopes in Precipitation Calculator" (OIPC) provides the monthly precipitations of δ^{2}H and δ^{18}O in function of geographic data (altitude, latitude and longitude). These data are corrected with the SMOW and are given in table 6 for the latitude 50°33'41" N, the longitude 4°41'56" E and the altitude 158 m, which corresponds to the coordinates of the field in Gembloux.

	Jan	Feb	Mar	Apr	**May**	**Jun**	Jul	Aug	Sept	Oct	Nov	Dec
δ^{2}H (‰)	-70	-72	-64	-52	**-37**	**-26**	-15	-20	-22	-41	-56	-66
δ^{18}O (‰)	-10	-10.2	-9.1	-7.5	**-5.5**	**-4.2**	-3.2	-3.0	-4.1	-6.5	-8.4	-9.5

Table 6: Isotopic composition in precipitaitons of ^{2}H and ^{18}O (corrected with the SMOW) for the specific location of the experiment, according to Bowen [Bowen G. J. and A., 2005].

4.5 Dual isotope plot

The analysis of the relationship between δ^2H and δ^{18}O is a preliminary requirement to the study of water stable isotopes. A linear relationship should be detected between the two isotopic compositions of oxygen and hydrogen [Barnes and Allison, 1988]. The relationship between δ^2H and δ^{18}O for each soil water samples and xylem sap water sample (plants) are shown in the dual isotope plot of the figure 24. Each color represents an experimentation date. The different symbols stand for each corresponding soil depth at which soil water samples have been extracted. The blue straight line is the representation of the Global Meteoric Water Line (GMWL).

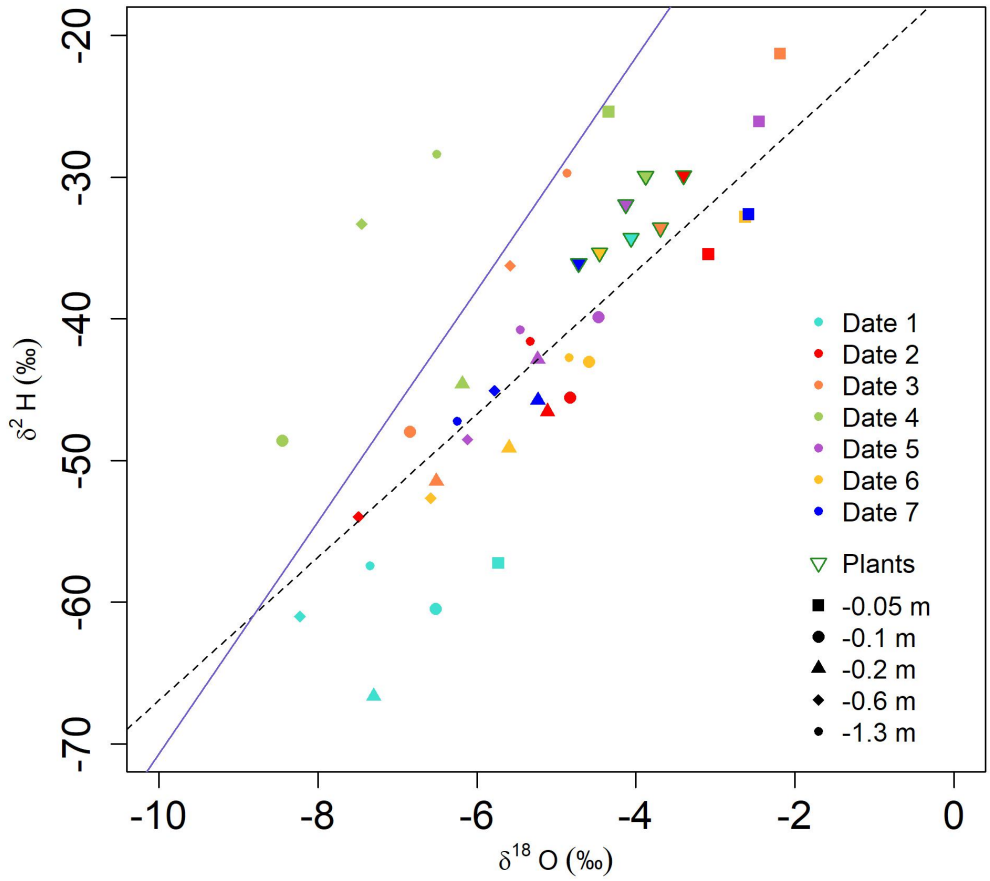

Figure 24: Dual isotope plot: relationship between δ^2H and δ^{18}O for each soil water samples and xylem sap water sample (plants) represented for each experimentation date. The different symbols represent each corresponding soil depth at which soil water samples have been extracted.

Globally, a linear relationship is found this dual isotope plot. The regression line of the dual isotope plot for all soil data is shown with the dashed line on figure 24, with the linear equation represented by

$$\delta^2 H = 5.05 \cdot \delta^{18} O - 16.45‰, \tag{20}$$

with a value of $R^2 = 0.76$ and p-value of 3.13 10^{-8}, meaning that the relationship is statistically very highly significant. This regression line does not take into account the isotopic information of Date 1 and Date 4, as we decided to discard them. Indeed, normally, a linear link should exist between both $\delta^2 H$ and δ^{18}O. However, for $\delta^2 H$ and δ^{18}O of Date 1 (in turquoise color) and 4 (in pale green), the graph (figure 24) reveals that no such link occurs. The low R^2 values for Date 1 and Date 4, available in the table 7, reinforce this statement. It is important that δ_{ti} lie on the frame of δ_s, for the significance of the data, but also because "Isotope mixing models cannot be solved if the values of the consumer lay outside the polygon defined by the sources in the two-dimensional isotope space, taking standard deviation into account (Phillips 2001)". Moreover, for Date 4, data are all above the GMWL. This situation is in reality impossible because data above the GMWL normally describe isotopic signature of water in the vapour phase. More details about the data's discrepancy of Date 1 and 4 are discussed in the next section. Table 7 summarizes every slope, intercept, R^2 and p-values (with the degree of significance in brackets) of the linear regressions concerning the δ_s of each date, as well as in the last line, concerning δ_{ti} of all dates.

Date	Data	Slope	Intercept	R^2	p-value
Date 1 (17/05)	δ_s	1.58	-49.52	0.15	0.5173
Date 2 (23/05)	δ_s	4.05	-23.69	0.87	0.02091
Date 3 (29/05)	δ_s	6.28	-4.67	0.86	0.0225
Date 4 (04/06)	δ_s	4.48	-6.56	0.46	0.2088
Date 5 (13/06)	δ_s	5.74	-12.4	0.95	0.00449
Date 6 (15/06)	δ_s	5.13	-19.2	0.98	0.000739
Date 7 (18/06)	δ_s	4.05	-22.6	0.96	0.00395
Date 1 to Date 7	δ_{ti}	4.4	-15.18	0.62	0.0349

Table 7: Linear regression's slope, intercept, R^2 and p-value of the regressions concerning the 5 δ_s of each date, as well as in the last line, concerning δ_{ti} of all dates.

4.6 RWU profiles using SIAR

Concerning the second part of this work, the objectives were the following: 1) Using the Stable Isotopes Analysis model in R (SIAR) in combination with stable isotopic compositions of crop xylem sap and soil water at different depths, we can determine the vertical root water uptake profile of winter barley in the field at different time steps. 2) The result of this vertical profile can be improved using Root Length Density data and soil moisture data.

4.6.1 No prior information in the model

At first, no prior information was inserted in the model to see the only influence of the isotopes on the RWU patterns outputs. Only Date 2, 3, 5, 6 and 7 are analysed due to abnormal data of Date 1 and 4.

The figure 25 shows the most frequent RWU proportion and its evolution through depth and time without prior insert in the model for δ_{ti} plant standard deviation of $\pm$ 1 or 2 ‰ (for O or H respectively) (left plot) and of $\pm$ 0.1 or 0.2 ‰ (right plot), as well as analytical standard deviation values for δ_s for both plots.

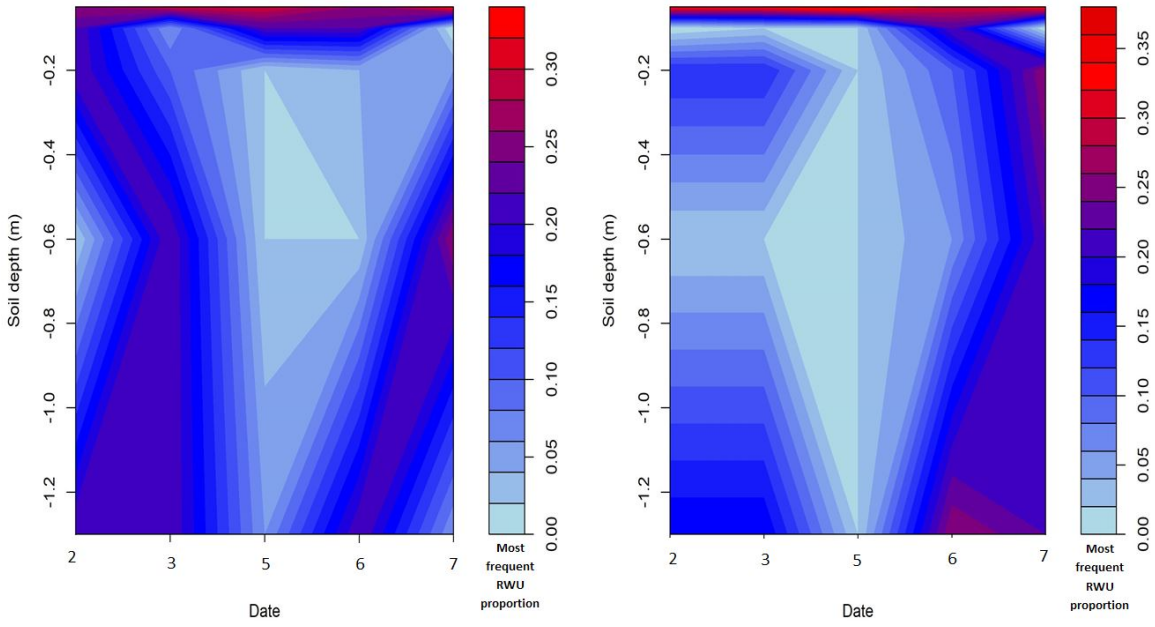

Figure 25: Most frequent RWU proportion and its evolution through depth and time without prior insert in the model. Values of plant standard deviation for δ_{ti} were equal to $\pm$ 1 or 2 ‰ (for O or H respectively) (left plot) and of $\pm$ 0.1 or 0.2 ‰ (for O or H respectively) (right plot), as well as analytical standard deviation values (less than 0.07‰ for O and less than 0.5‰ for H) concerning δ_s for both plots.

In addition, the model ran with different types of standard deviations for the plant δ_{ti} ($\pm$ 1 or 2 ‰ for O or H, and $\pm$ 0.1 or 0.2‰ for O or H), and with values of standard deviations equal to $\pm$ 1 or 2‰ for δ_s (figure 26). The standard deviations for H are always doubled compared to the one of O.

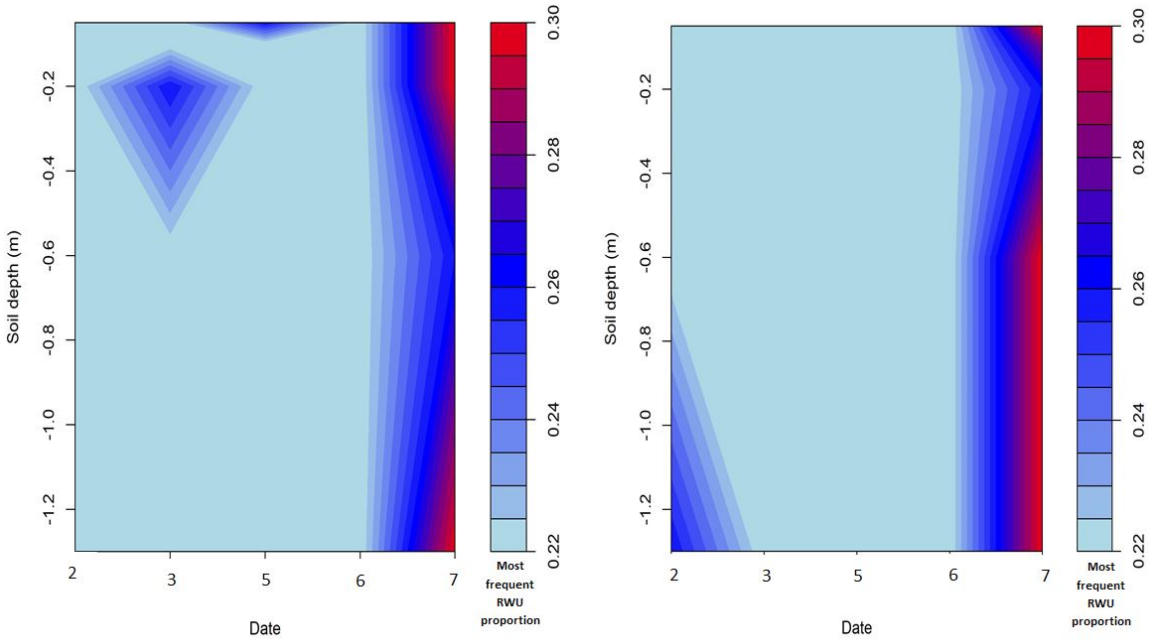

Figure 26: Most frequent RWU proportion and its evolution through depth and time without prior insert in the model for δ_{ti} plant standard deviation of $\pm$ 1 or 2‰ (left plot) and of $\pm$ 0.1 or 0.2‰ (right plot), and with a value of standard deviation of $\pm$ 1 or 2‰ for δ_s for both plots.

By modifying standard deviation values, the sensibility of the model to δ_s standard variation has been tested. The graph of the figure 26 shows that the model is not able to differentiate each source when the standard deviation of δ_s is too important. Each depth has almost the same value of most frequent RWU proportion.

4.6.2 Prior information in the model

This time, prior information (based on RLD and SWC) was inserted in the model in order to guide the RWU proportions. Graphs are given in order to discuss the possible improvement of the RLD and SWC to RWU study. . The figure 27 shows the most frequent RWU proportion and its evolution through depth and time for the different standard deviations values concerning δ_{ti} ($\pm$ 1 or 2 ‰ and $\pm$ 0.1 or 0.2 ‰) and δ_s (analytical errors and $\pm$ 1 or 2 ‰).

We can see that the most frequent RWU proportion is relatively steady through time. In addition, the model is not sensitive to a variation of standard deviation for both δ_{ti} and δ_s.

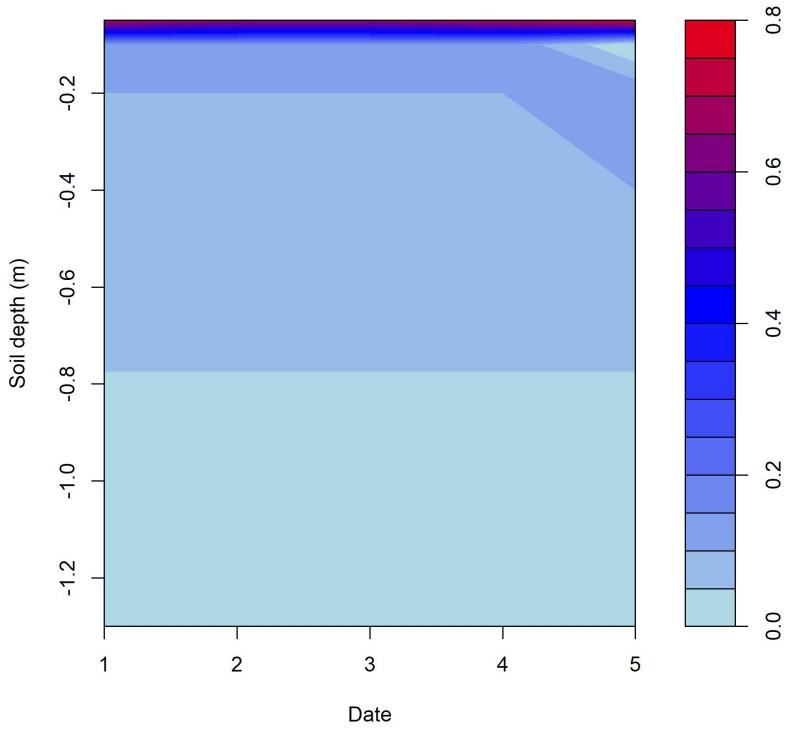

Figure 27: Most frequent RWU proportion and its evolution through depth and time with RLD and SWC used as prior information in the model. This graph results from different standard deviation inserted in the model: $\pm$ 1 or 2 ‰ or $\pm$ 0.1 or 0.2 ‰ for δ_{ti} and $\pm$ 1 or 2 ‰ or analytical errors for δ_s.

The values of p_j, the prior vector for each time calculated on the base of equation (18), is given on figure 28. The similarities between this graph and the one of the most frequent RWU proportion (figure 27) are evident. Because p_j represents a relative proportion for each depth, the sum of p_j for each depth equals one. Concerning Date 7, only four depths are concerned, instead of five. That is why the p_j vector is distributed between the four depths, so that at -0.05 m, the value of p_j is increased to 0.81 instead of 0.68 for previous dates. At 1.3 m deep, the graph shows a p_j value near zero, it is in reality equals to 0.01.

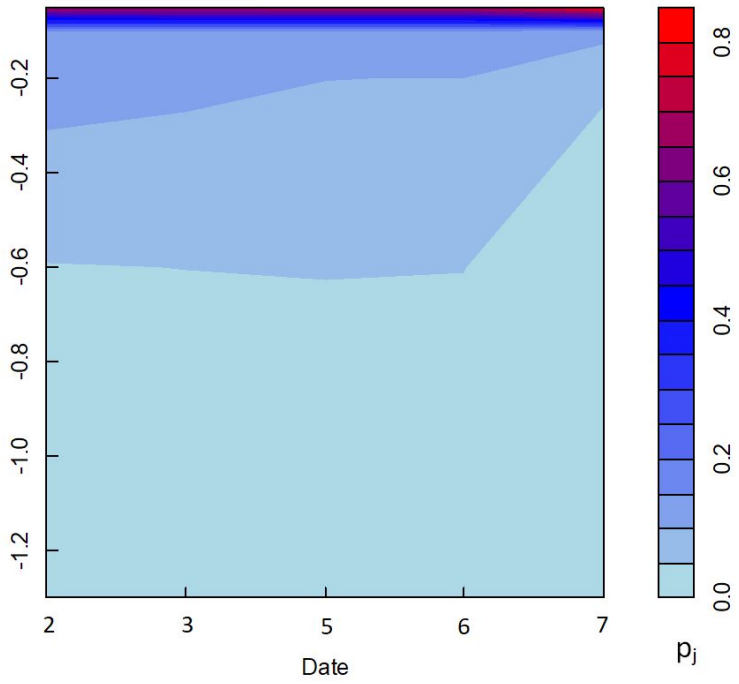

Figure 28: Value of p_j, the prior vector for each time calculated on the base of equation (18).

4.6.3 SWC and pF evolutions through depth and time

The evolution of the pF and the SWC with depth and time are shown on the two graphs of the figure 29. The pF values follow the trend of the SWC since it derives from it. pF values are calculated based on the pF curves of each soil layer. The scales of the two graphs are reversed in order to better see this effect. The higher the pF, the lower the SWC.

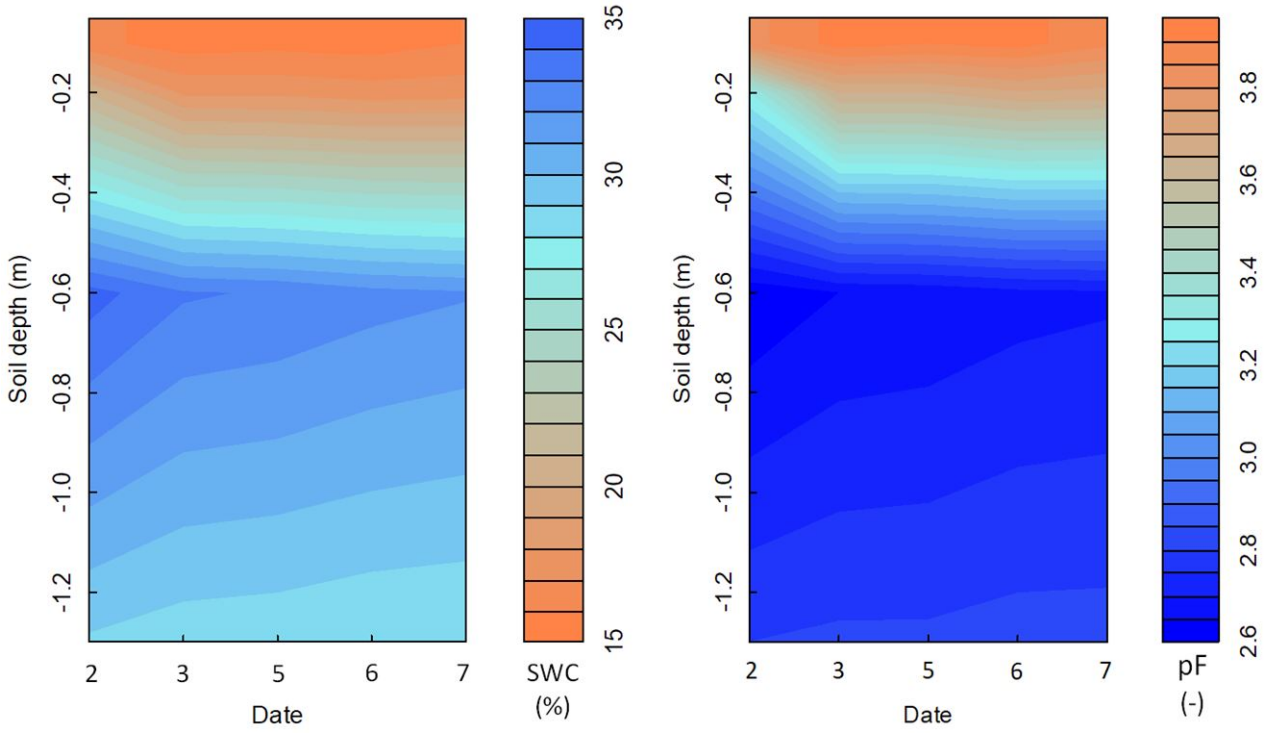

Figure 29: Evolution of the SWC (left plot) and of pF values (right plot) through depth and time, considering each experimentation date.

5 Discussion

The first objective of this work was to adjust a method of soil water isotopes monitoring (Rothfuss et al.) and to test its viability in the field. The second objective was to test its ability to retrieve representative RWU patterns.

5.1 Evaluation of the method of soil water vapour extraction from the soil

Quantitatively, results of the successive experiments have demonstrated that enough water vapour can be harvested under field conditions to measure the isotopic concentrations with a laser spectrometer (figure 18). This study has shown that each entry hole of the traps should be analysed prior to the extraction in order to avoid any obstruction by the high vacuum grease (as happened for Date 7).

Qualitatively speaking, the soil water isotopic compositions were not all exploitable. Some data (of Date 1 and Date 4) had to be discarded. Their position in the dual isotope plot indicated the non sense of their value. In the case of Date 1, the irrelevance of the data is explained in the next subsection (5.2). Concerning Date 4, the irrelevance of the data can be explained by a possible ambient air contamination. This could be due to a sealing problem at or before the level of the traps. Indeed, each time, the Swagelok® fittings were manually closed. So this step could lead to a sealing issue. In addition, the air relative humidity was relatively high during the field experiment this day (see figure 20).

5.1.1 Viability of the system deployed in the field

From the 16^{th} of April to the 10^{th} of July, 15 permeable tubes remained underground from 0.05 m to 1,3 m deep. The whole system resisted through time and to the outside weather. After a three month period, the underground system was found to be at the same place and no significant displacement of the tubes had occurred.
Nevertheless, the Swagelok® fittings that linked the permeable tubes to 6 mm polyethylene composite tubing Synflex® had slightly moved from their original position. In the case of a similar experiment that would take place in a longer time frame, particular attention should be given to the fixing system that tends to slack with time.

5.1.2 Logistical considerations

In order to ease the experiment's implementation, some logistical considerations must to be taken into account to select the best suited location. For instance, it is necessary to have enough space to be able to use the water extraction system

without damaging the plants but also to store all the necessary material of the extraction system. In this context, the wood strip, adjacent to our experimentation field, was useful because it provided enough space for the experimenter and its material. Moreover, the shade provided by trees decreased the heating effect of the sun, and therefore the speed of dry ice sublimation that may affect the water trap. Another consideration is the accessibility to the site. For example, the proximity of a paved road allowed to bring all the equipment close to the experimentation site while diminishing the risk of damaging fragile devices that were used before and after each data intake.

5.2 Evaluation of the method of soil water extraction from the traps

The method using gas permeable tubing was tested in one location of a winter barley field. It was combined with cold cryogenic traps and a water recovery system in laboratory. This latter laboratory work required the use of a hotgun and dry ice in order to collect the totality of the water in the trap. This method was tested from Date 2 to Date 7.

We also wanted to test the potential effects of setup changes on measurements of the soil isotopic composition. A simpler method was tested to see if it could be considered as rigorous enough to avoid some fractionation problems during the water extraction from the trap. The method did not rely on the use of the hotgun to recover all the water from the trap. The hypothesis was based on the fact that with a larger water quantity collected, the fractionation effect could potentially decrease. This has been tested for Date 1. There is no doubt that this simplest protocol is not rigorous enough since condensated water remained on the edges of the trap. This effect is visible on the left picture of figure 30. The condensate water on the edges of the trap is impossible to collect and therefore the isotopic signature of the water sample does not reflect the total isotopic signature of the water sample. The risk of fractionation is effectively too high using the simplified procedure, even if bigger amounts of water were harvested. The position of the data in the dual plot reinforced this statement since no linear relationship between $\delta^2 H$ and δ^{18}O was found, with a R^2 equals to 0.15. This simplest water extraction protocol is therefore not suitable to the analysis of water stable isotopes.

From Date 2 to Date 7, the trap water was collected manually with the help of the hotgun, without using the extraction line of Jülich. The extraction operation remains tricky but at the end, visually, the result appeared to be rigorous enough. The result of the operation can be seen on the figure 30. This operation to collect all the water at the bottom of the trap takes approximately one hour each trap/depth.

The results in the dual isotope plot revealed a significant correlation between $\delta^{18}O$ and $\delta^{2}H$ (R^2 of 0.76). This R^2 could increase if more attention would be given to the risks of contamination due to sealing problems.

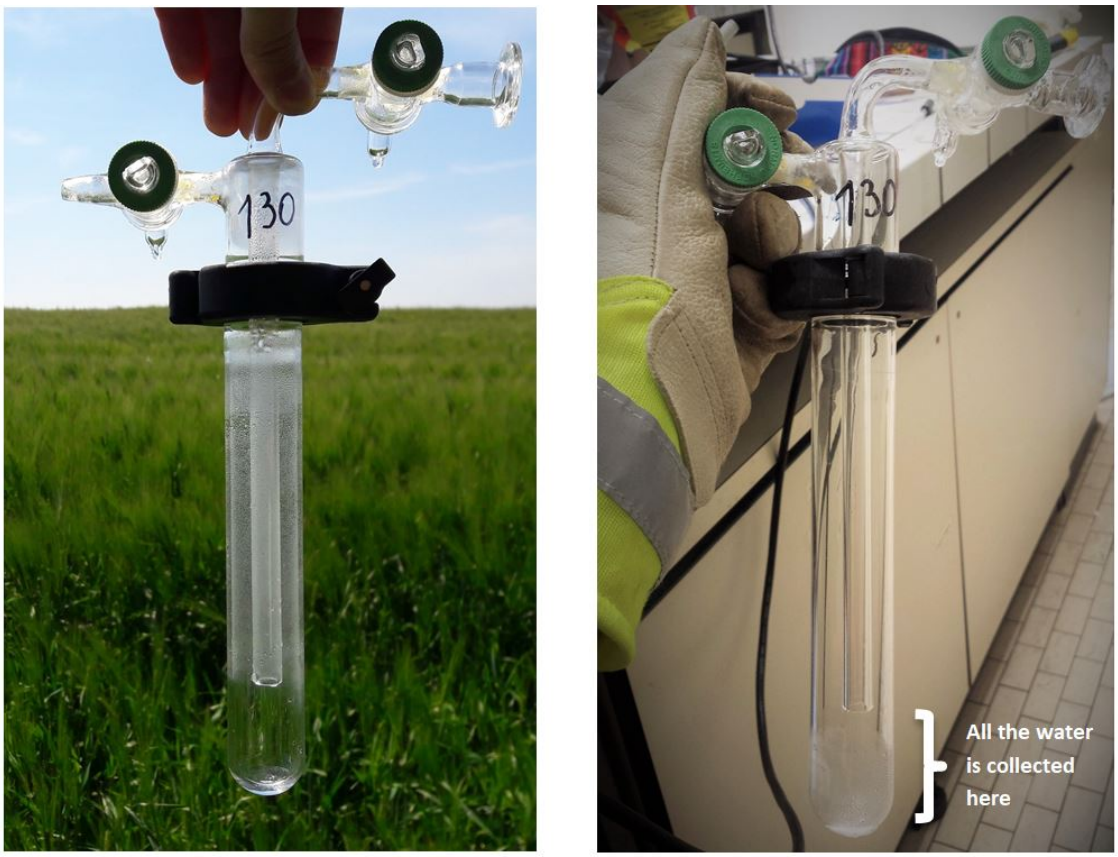

Figure 30: Comparison of the trap just after the field extraction (left picture) and after the laboratory part with the hotgun (right picture). Evidence of water mobilisation at the bottom of the trap is visible.

As shown in the results, values of $\delta^{18}O$ and $\delta^{2}H$ through depth are shifted from one date to another one. These variations could not be entirely due to a natural variation in time. Therefore we might suspect a fractionation problem due to the field or/and laboratory extraction process.

Some inherent errors occur during the sampling of the isotopic data (sources or consumers) [Hopkins and Ferguson, 2012]. For example, the possible contamination of the air moisture on the extracted plant tillers exists. This effect may lead to fractionation and so increase the standard deviation of the δ_{ti}.

5.3 Challenges, limitations and advantages of the method

"Isotopic composition of water is inherently prone to fractionation. This serves as a scientific advantage by providing discrete signatures to various pools but also a challenge to successfully maintain consistent water signature from collection to isotopic analysis" [Berry et al., 2018].

The analyses of the isotopic composition of soil water is done offline in laboratory. Therefore there is an important time lag from the sampling to the data acquisition [Herbstritt et al., 2012]. This makes the adaptation of the experimental protocol more challenging if anomalies appear in the data.

The offline analysis of the water samples renders the process highly time-consuming. For this reason, the number of data acquired is low compared to a continuous isotopic monitoring as done in laboratory. As a result of a low data acquisition's frequency, data's reliability is subsequently reduced. In addition it makes it more difficult to study processes having a high variability in time and space, such as the RWU [Rothfuss and Javaux, 2017].

The necessary labour both in field and lab is considerable. In average, two days were necessary to obtain measures of one day.

A significant advantage of the method is the non destructive aspect of the in-situ measurements. A benefit resulting from this advantage is the capacity of the method to sample simultaneously at different depths. In addition, once installed, no maintenance was required to keep the system available between the experiments. Except the fact that it was necessary to check stocks of CO_2 and dry air bottles. It can still be considered as a significant advantage compared to other methods.

5.4 Retrieving relative RWU profiles of winter barley

The second main objective of this work was to retrieve RWU profiles from water stable isotopic data and through the use of the SIAR model. The inputs of the model are first discussed before the examination of the outputs of the model. We have tested if the results can be improved using RLD data and SWC.

The spatial and time limitations of the study is first to underlined, especially because RWU highly changes in time and space [Marshall et al., 2007]. Actually, it is essential to spatially cover every potential sources of RWU [Sprenger et al., 2016]. Even so, in this study, the deepest soil layer possibly contributing to RWU was 1.3 m deep. This depth is sufficient for the study of winter barley, since almost no more roots were found at this depth.

5.4.1 Model inputs

It is important to realise that "SIAR will always try to fit a model even if the data are nonsensical" [Inger et al., 2010]. Therefore the analysis of the input data prior to the model run is indispensable.

In natural conditions, the upper and downward limits are not controlled. On the one hand, precipitations play a key role in the variation of δ_s and impose an upper-limit condition. Isotopic compositions of the precipitations (δ_{pp}), that are given in the table 6, equal in average -44.5 ‰ (for δ^2H) and -6.5 ‰ (for $\delta^{18}O$) respectively for May and June. These data are consistent with values of δ_s (graph of the figure 23). In the soil's upper layer, δ_s are slightly enriched compared to δ_{pp}, because of the evaporation process occurring at the soil interface. As a reminder, every experiment took place a few days or the day after a rain event. It reinforces the reliability of the data on which the model is based on. Furthermore, δ_{pp} varies considerably with time due to seasonality effect as explained in the literature [Sprenger et al., 2016]. On the other hand, concerning the lower-limit condition, this one is in this case imposed by the water table. The fact that the isotopic composition increases 1.3 m deep indicates the likely presence of a water table. This water table is less enriched isotopically. This leads to profiles that are left shifted with depth. The effect of the water table on the isotope profile decreases for Date 7, while its SWC is also less important than earlier. In this case, the δ of the water table is comparable to the δ of the summer precipitations.

An important isotope gradient occurs near the surface, while more deeper, this gradient tends to decrease. This statement is consistent with the scientific literature [Barnes and Allison, 1988, Mook and Rozanski, 2000, Rothfuss and Javaux, 2017]. If more depths were investigated, we would probably see better an exponential shape of δ_s through depth. We can however notice that there are only small differences in the sources signature. For this reason, before running the model, one would expect that the discriminatory power of the model could decrease.

From the view of the two bottom graphs of the figure 23, δ_{ti} of each date seems to be a compromise between the first, second and third depth, where the root density is the highest. This shows that isotopic approach could be a valuable tool to retrieve RWU.

5.4.2 Model outputs

As expected before running the model, the output data are influenced by the input data, that are in this case not enough discriminative. On the one hand, the choice

of isotopic analysis may be unsuitable if there is only a small variation within δ_s [Bond and Diamond, 2011, Phillips et al., 2014]. On the other hand, a less important number of sources may ease the differentiation of each contributions by the model [Moore and Semmens, 2008]. The "Best practices for use of stable isotope mixing models" already outlined the importance of this issue, leading to a "too diffuse" solutions, (referring to the density curves) [Phillips et al., 2014]. From the output of the model without prior, we can conclude that the sources are not enough distinguishable from each other.

The model is being only statistically based and no ecological data are input in this scenario. The fact that the model predicts a RWU at 1.3 m deep is not likely to occur since almost no more roots were found so deep. Indeed, the model can hardly differentiate δ_s at 1.3 m and 0.2 m deep because their isotopic signature are very close. The presence of the water table is in this case harmful to the ability of the model to retrieve RWU.

The sensibility test of the model to standard variation showed that the larger the standard deviation, the more the model struggles to identify the most frequent RWU proportion. When the standard deviation of δ_{ti} varied from 0.1 or 0.2 $‰$ to 1 or 2 $‰$, the model could provide different RWU patterns, even tough less likely to occur. However, when the standard deviation of δ_{ti} varied from the analytical values to 1 or 2 $‰$, the model could hardly provide a result dissociated from the prior information. Indeed, it provided solutions almost equal for each depth.

The run of the model with prior information showed that data were definitely too constrained by the prior information. This effect can be explained by the fact that the model can hardly differentiate the different δ_s. Input data are not enough differentiable, so that the model highly rely on the prior information and is too constrained by them. Even changes of the standard deviations for both δ_s and δ_{ti} were not taken into account by the model.

Even tough the SWC is different for each time step, the RLD is fixed in time. However, the SWC only varies slightly. Therefore the value of p_j is almost fixed in time. This can be seen on the graph of figure 28. It explains that the outputs are almost static in time, because they are too influenced by the priors.

5.4.3 Ecological interpretations

The model intended to shed light on the most frequent RWU proportions across depths.

We have seen that the crop takes out the water from the soil mainly in the first 0.8 m of the soil, with highest extractions near the soil surface. If we look at the upper part of the graph of the figure 25, it is clear that the model without prior predicts that more water are taken from this depth range. Furthermore, the model with prior information predicts it too, but with even more water extracted near the soil surface. Although more water stress is observable in this zone.

At the same time, the pF values lies on the available water range all along the experiment because it is always comprised between 2 and 4.2 (between the FC and the PWP). We can see on the graph of the figure 29 that the soil is dryer near the surface and so the pF increases in this zone. The pF curves given in the section 3.1.4 show that each soil layer has different response in terms of water retention. A clay accumulation is observed lower in the profile, translated by a higher retention capacity. Indeed, the structure plays a key role in the way the soil is able to retain water, that will be in turn available for plants. We can assume in this case that the availability of water does not negatively affect the capacity of the plants to extract soil water.

The loamy soil, which is representative of the soils of the Hesbaye region, has high agronomic potential since the retention capacity is relatively high. This soil type is not limiting to the RWU of winter barley during its grain development and its grain ripening stage.

It is important to underline that precautions must be taken in the analysis of these data. In fact, fractionation problems during the sampling, as well as the too low gradient of δ_s renders the output data less reliable. Moreover, the spatial heterogeneity can be high, especially in this field regarding past land use activities. Therefore repetitions at different locations are necessary to draw up conclusions with respect to the RWU profiles in general.

In conclusion and despite the high uncertainty, SIAR could provide valuable insights on the RWU pattern in a location of the field.

6 Outlook

The simple approach of the model only allowed a two dimensional study. This simpification ignores water lateral flows and root dynamics that evolve in reality in three dimensions. Recent advances have made possible the study of such processes in three dimensions, while considering the root system as a whole [Dunbabin et al., 2013]. The need to couple the experiment-modeling approach has already been pointed out [Rothfuss and Javaux, 2017]. Therefore, the combination between a physically based model to the isotopic approach could be further investigated.

From a logistical viewpoint, the method renders difficult the possibility to increase the number of sources. At the same time, it is worth remembering that a model is a simplification of the reality. In this context, a greater number of soil depths could be included in a further study.

Ideally, repetitions of the experiment should be put in place at different locations in the field, on the one hand to give robustness to the results, and on the other hand to potentially analyse the influence of local environmental parameters on the soil method extraction.

This study, as most studies in soil isotopic measurements, took the opportunity to trace naturally the water stable isotopes to retrieve RWU. However, it is possible to apply a label water pulse in the soil to force the water tracking. This could provide a valuable tool to more precisely trace the RWU, as explained in a paper of Moreira [Moreira et al., 2000]. In addition, this could render more distinctive the different water sources, and lead to a better readings of the input data from the model.

One of the outlooks regarding research in RWU would be to apply the method to agroforestry and/or plants association studies. Indeed, these agricultural practices are of a major importance to face critical issues such as climate change.

The measure of the field RLD is a meticulous process, that could only be applied to last stage of winter barley in the present study. However, the study of the root dynamics is a key process in RWU analysis. As a further research, it would be interesting to obtain RLD for every development stages of the winter barley. In addition, a study focused on the entire crop cycle would be relevant to put in place, as winter barley already develops its roots system in the winter season.

7 Conclusion

Soil water has long been extracted in a destructive manner for the purpose of water stable isotopes studies. This work was conducted to provide insights on a non-destructive (but invasive) soil water vapour extraction method applied in the field, a promising technique in the isotopic scientific research.

This work has demonstrated that the gas permeable tubing method is working properly in the field and provides sufficient water quantities to be analysed with a laser spectrometer. A significant linear correlation was found between δ^2H and δ^{18}O. However, slight fractionation issues occurred (once during the field and once during the lab extraction).

Ultimately, this method offers great perspectives if the gas-permeable tubes are combined with an online laser spectrometer to measure in situ δ_s. Indeed, on the contrary to the offline isotopic measurement, this alternative could offer several advantages such as high frequency measurements and a more time and labour effective method.

Isotopic approach is a valuable tool to trace environmental changes, such as RWU process. In this work, we have considered the RWU as a non-fractionating process in order to assume that the δ_{ti} is representative of the δ_s of the water extracted by roots in soil. We also have considered isotopic thermodynamic equilibrium between soil liquid water and soil water vapour.

In this research, we have demonstrated that input data are of critical importance when using multi-sources mixing model. Indeed, the model could hardly differentiate the different sources that were in this case not enough discriminative. As a result, we have touched at the core of the limits of the model since the model provided MFV with a high level of uncertainty. On the other hand, when prior information (considering the RLD and the SWC) is inserted in the model, the results are definitely too constrained. In general, the model could provide insights on RWU process, a key process remaining challenging to measure. In view of improving the discriminative power of the model, it is possible to apply a label water (enriched or depleted in heavy isotopes) in the soil to force the water tracking.

In conclusion, this study has shown that it is essential to include ecological data such as the RLD and the SWC in SIAR, with enough attention given to sufficiently discriminative data. The RLD and the SWC are also important elements for the SIAR result interpretation.

References

[Goo, 2018] (2018). Google earth https://www.google.com/earth/. *Website*.

[wal, 2018] (2018). Géoportail de wallonie http://geoportail.wallonie.be/walonmap. *Website*.

[Allison et al., 1983] Allison, G. B., Barnes, C. J., and Hughes, M. W. (1983). The distribution of deuterium and18O in dry soils 2. Experimental. *Journal of Hydrology*, 64(1-4):377–397.

[Baize and Girard, 2008] Baize, D. and Girard, M. (2008). Référentiel pédologique–association française pour l'étude des sol. *Editions Quae*.

[Barnes and Allison, 1988] Barnes, C. and Allison, G. (1988). Tracing of water movement in the unsaturated zone using stable isotopes of hydrogen and oxygen. *Journal of Hydrology*, 100(1-3):143–176.

[Bernard Delcambre, 2002] Bernard Delcambre, J.-L. P. (2002). Carte géologique de wallonie, notice exlicative pour la région de chastre-gembloux. *Unité de Géologie, Université catholique de Louvain*.

[Berry et al., 2018] Berry, Z. C., Evaristo, J., Moore, G., Poca, M., Steppe, K., Verrot, L., Asbjornsen, H., Borma, L. S., Bretfeld, M., Hervé-Fernández, P., et al. (2018). The two water worlds hypothesis: Addressing multiple working hypotheses and proposing a way forward. *Ecohydrology*, 11(3):1843.

[Bond and Diamond, 2011] Bond, A. L. and Diamond, A. W. (2011). Recent bayesian stable-isotope mixing models are highly sensitive to variation in discrimination factors. *Ecological Applications*, 21(4):1017–1023.

[Bowen, 1985] Bowen, G. (1985). Roots as a component of tree productivity. *Attributes of trees as crop plants*, pages 303–315.

[Bowen, 2018] Bowen, G. (2018). The online isotopes in precipitation calculator, http://wateriso.utah.edu/waterisotopes/.

[Bowen et al., 2007] Bowen, G. J., Cerling, T. E., and Ehleringer, J. R. (2007). Stable isotopes and human water resources: signals of change. *Terrestrial Ecology*, 1:283–300.

[Bowen G. J. and A., 2005] Bowen G. J., W. L. I. and A., H. K. (2005). Global application of stable hydrogen and oxygen isotopes to wildlife forensics. *Oecologia*, pages 337–348.

[Clinton et al., 2004] Clinton, B. D., Vose, J. M., Vroblesky, D. A., and Harvey, G. J. (2004). Determination of the relative uptake of ground vs. surface water by populus deltoides during phytoremediation. *International journal of phytoremediation*, 6(3):239–252.

[Colinet, 2003] Colinet, G. (2003). *Éléments traces métalliques dans les sols-Contribution à la connaissance des déterminants de leur distribution spatiale en région limoneuse belge*. PhD thesis, Thèse, Université de Gembloux, Belgique.

[Craig, 1961] Craig, H. (1961). Isotopic variations in meteoric waters. *Science*, 133(3465):1702–1703.

[Dalton, 1989] Dalton, F. (1989). Plant root water extraction studies using stable isotopes. In *Structural and functional aspects of transport in roots*, pages 151–155. Springer.

[Dawson et al., 2002] Dawson, T. E., Mambelli, S., Plamboeck, A. H., Templer, P. H., and Tu, K. P. (2002). Stable isotopes in plant ecology. *Annual review of ecology and systematics*, 33(1):507–559.

[Degré, 2017] Degré, A. (2017). Cours de modélisation des transferts dans les biosystèmes, master 1. *Gembloux Agro Bio-Tech*.

[Devices, 2017] Devices, D. (2017). 5tm water content and temperature sensors. *Manual*.

[Dubbert et al., 2013] Dubbert, M., Cuntz, M., Piayda, A., Maguás, C., and Werner, C. (2013). Partitioning evapotranspiration – Testing the Craig and Gordon model with field measurements of oxygen isotope ratios of evaporative fluxes. 496:142–153.

[Dunbabin et al., 2013] Dunbabin, V. M., Postma, J. A., Schnepf, A., Pagès, L., Javaux, M., Wu, L., Leitner, D., Chen, Y. L., Rengel, Z., and Diggle, A. J. (2013). Modelling root–soil interactions using three–dimensional models of root growth, architecture and function. *Plant and soil*, 372(1-2):93–124.

[Ehleringer and Dawson, 1992] Ehleringer, J. and Dawson, T. (1992). Water uptake by plants: perspectives from stable isotope composition. *Plant, Cell & Environment*, 15(9):1073–1082.

[Fabre et al., 2003] Fabre, F., Dedryver, C.-A., Leterrier, J., and Plantegenest, M. (2003). Aphid abundance on cereals in autumn predicts yield losses caused by barley yellow dwarf virus. *Phytopathology*, 93(10):1217–1222.

[Gangi et al., 2015] Gangi, L., Rothfuss, Y., Ogée, J., Wingate, L., Vereecken, H., and Brüggemann, N. (2015). A new method for in situ measurements of oxygen isotopologues of soil water and carbon dioxide with high time resolution. *Vadose zone journal*, 14(8).

[Gat, 2010] Gat, J. (2010). *Isotope hydrology: a study of the water cycle*, volume 6. World scientific.

[Gat, 1996] Gat, J. R. (1996). Oxygen and hydrogen isotopes in the hydrologic cycle. *Annual Review of Earth and Planetary Sciences*, 24(1):225–262.

[Gat et al., 2001] Gat, J. R., Mook, W. G., and Meijer, H. A. (2001). Environmental isotopes in the hydrological cycle. *Principles and Applications UNESCO/IAEA Series*, 2:63–7.

[Greaves et al., 1996] Greaves, R. J., Lesmes, D. P., Lee, J. M., and Toksöz, M. N. (1996). Velocity variations and water content estimated from multi-offset, ground-penetrating radar. *Geophysics*, 61(3):683–695.

[Gregory, 2008] Gregory, P. J. (2008). *Plant roots: growth, activity and interactions with the soil*. John Wiley & Sons.

[Hagemann et al., 1970] Hagemann, R., Nief, G., and Roth, E. (1970). Absolute isotopic scale for deuterium analysis of natural waters. absolute d/h ratio for smow. *Tellus*, 22(6):712–715.

[Hallet, 2015] Hallet, V. (2015). *Itinéraire de la Vallée de l'Orneau: Sentiers géologiques et pédologiques en Province de Namur*. Presses universitaires de Namur.

[Herbstritt et al., 2012] Herbstritt, B., Gralher, B., and Weiler, M. (2012). Continuous in situ measurements of stable isotopes in liquid water. *Water Resources Research*, 48(3).

[Hopkins and Ferguson, 2012] Hopkins, J. B. and Ferguson, J. M. (2012). Estimating the diets of animals using stable isotopes and a comprehensive bayesian mixing model. *PLoS One*, 7(1):28478.

[Horita et al., 2008] Horita, J., Rozanski, K., and Cohen, S. (2008). Isotope effects in the evaporation of water: a status report of the craig–gordon model. *Isotopes in environmental and health studies*, 44(1):23–49.

[Horrigan et al., 2002] Horrigan, L., Lawrence, R. S., and Walker, P. (2002). How sustainable agriculture can address the environmental and human health harms of industrial agriculture. *Environmental health perspectives*, 110(5):445.

[Inger et al., 2010] Inger, R., Jackson, A., Parnell, A., and Bearhop, S. (2010). Siar v4 (stable isotope analysis in r). an ecologist's guide.

[Khaldoun et al., 1990] Khaldoun, A., Chery, J., and Monneveux, P. (1990). Étude des caractères d'enracinement et de leur rôle dans l'adaptation au déficit hydrique chez l'orge (hordeum vulgare l). *Agronomie*, 10(5):369–379.

[Kotz and Treichel Jr, 2006] Kotz, J. C. and Treichel Jr, P. M. (2006). *Chimie générale*. De Boeck Supérieur.

[Lobet et al., 2014] Lobet, G., Couvreur, V., Meunier, F., Javaux, M., and Draye, X. (2014). Plant water uptake in drying soils. *Plant Physiology*, 164(4):1619–1627.

[Macaigne, 2011] Macaigne, P. (2011). Stable isotopes, their use in soil hydrology. *Encyclopedia of agrophysics*, pages 849–854.

[Mahindawansha et al., 2018] Mahindawansha, A., Orlowski, N., Kraft, P., Rothfuss, Y., Racela, H., and Breuer, L. (2018). Quantification of plant water uptake by water stable isotopes in rice paddy systems. *Plant and Soil*, pages 1–22.

[Majoube, 1971] Majoube, M. (1971). Fractionnement en oxygene 18 et en deuterium entre l'eau et sa vapeur. *Journal de Chimie Physique*, 68:1423–1436.

[Marshall et al., 2007] Marshall, J. D., Brooks, J. R., and Lajtha, K. (2007). Sources of variation in the stable isotopic composition of plants. *Stable isotopes in ecology and environmental science*, 2:22–60.

[Mook and Rozanski, 2000] Mook, W. and Rozanski, K. (2000). Environmental isotopes in the hydrological cycle. *IAEA Publish*, 39.

[Moore and Semmens, 2008] Moore, J. W. and Semmens, B. X. (2008). Incorporating uncertainty and prior information into stable isotope mixing models. *Ecology letters*, 11(5):470–480.

[Moreira et al., 2000] Moreira, M. Z., da SL Sternberg, L., and Nepstad, D. C. (2000). Vertical patterns of soil water uptake by plants in a primary forest and an abandoned pasture in the eastern amazon: an isotopic approach. *Plant and Soil*, 222(1-2):95–107.

[Ogle et al., 2004] Ogle, K., Wolpert, R. L., and Reynolds, J. F. (2004). Reconstructing plant root area and water uptake profiles. *Ecology*, 85(7):1967–1978.

[Orlowski et al., 2016] Orlowski, N., Pratt, D. L., and McDonnell, J. J. (2016). Intercomparison of soil pore water extraction methods for stable isotope analysis. *Hydrological Processes*, 30(19):3434–3449.

[Pallardy, 2010] Pallardy, S. G. (2010). *Physiology of woody plants*. Academic Press.

[Parnell and Inger, 2016] Parnell, A. and Inger, R. (2016). Stable isotope mixing models in r with simmr.

[Parnell et al., 2010] Parnell, A. C., Inger, R., Bearhop, S., and Jackson, A. L. (2010). Source partitioning using stable isotopes: coping with too much variation. *PloS one*, 5(3):e9672.

[Parnell et al., 2013] Parnell, A. C., Phillips, D. L., Bearhop, S., Semmens, B. X., Ward, E. J., Moore, J. W., Jackson, A. L., Grey, J., Kelly, D. J., and Inger, R. (2013). Bayesian stable isotope mixing models. *Environmetrics*, 24(6):387–399.

[Phillips and Gregg, 2001] Phillips, D. L. and Gregg, J. W. (2001). Uncertainty in source partitioning using stable isotopes. *Oecologia*, 127(2):171–179.

[Phillips et al., 2014] Phillips, D. L., Inger, R., Bearhop, S., Jackson, A. L., Moore, J. W., Parnell, A. C., Semmens, B. X., and Ward, E. J. (2014). Best practices for use of stable isotope mixing models in food-web studies. *Canadian Journal of Zoology*, 92(10):823–835.

[Romano and Santini, 2002] Romano, N. and Santini, A. (2002). 3.3. 3 field. *Methods of Soil Analysis: Part 4 Physical Methods*, (methodsofsoilan4):721–738.

[Rothfuss, 2017] Rothfuss, Y. (2017). Cours de relations plantes-écosystèmes-climat, master 2. *Gembloux Agro Bio-Tech*.

[Rothfuss et al., 2010] Rothfuss, Y., Biron, P., Braud, I., Canale, L., Durand, J.-L., Gaudet, J.-P., Richard, P., Vauclin, M., and Bariac, T. (2010). Partitioning evapotranspiration fluxes into soil evaporation and plant transpiration using water stable isotopes under controlled conditions. *Hydrological processes*, 24(22):3177–3194.

[Rothfuss and Javaux, 2017] Rothfuss, Y. and Javaux, M. (2017). Reviews and syntheses: Isotopic approaches to quantify root water uptake: a review and comparison of methods. *Biogeosciences*, 14(8):2199.

[Rothfuss et al., 2015] Rothfuss, Y., Merz, S., Vanderborght, J., Hermes, N., Weuthen, A., Pohlmeier, A., Vereecken, H., and Brüggemann, N. (2015). Long-term and high-frequency non-destructive monitoring of water stable isotope profiles in an evaporating soil column. *Hydrology and Earth System Sciences*, 19(10):4067–4080.

[Rothfuss et al., 2013] Rothfuss, Y., Vereecken, H., and Brüggemann, N. (2013). Monitoring water stable isotopic composition in soils using gas-permeable tubing and infrared laser absorption spectroscopy. *Water resources research*, 49(6):3747–3755.

[Smit et al., 2013] Smit, A. L., Bengough, A. G., Engels, C., van Noordwijk, M., Pellerin, S., and van de Geijn, S. (2013). *Root methods: a handbook*. Springer Science & Business Media.

[Soderberg et al., 2012] Soderberg, K., Good, S. P., Wang, L., and Caylor, K. (2012). Stable isotopes of water vapor in the vadose zone: A review of measurement and modeling techniques. *Vadose Zone Journal*, 11(3).

[Sprenger et al., 2016] Sprenger, M., Leistert, H., Gimbel, K., and Weiler, M. (2016). Illuminating hydrological processes at the soil vegetation atmosphere interface with water stable isotopes. *Reviews of Geophysics*, 54(3):674–704.

[Stumpp et al., 2018] Stumpp, C., Brüggemann, N., and Wingate, L. (2018). Stable isotope approaches in vadose zone research. *Vadose Zone Journal*, 17(1).

[Sun et al., 2009] Sun, X., Chen, J., Tan, H., Rao, W., Wang, Y., Liu, X., and Su, Z. (2009). Study on the mechanism of isotope fractionation in soil water during the evaporation process under equilibrium condition. *Chinese Journal of Geochemistry*, 28(4):351–357.

[Tyree and Ewers, 1991] Tyree, M. T. and Ewers, F. W. (1991). The hydraulic architecture of trees and other woody plants. *New Phytologist*, 119(3):345–360.

[UMS, 2013] UMS (2013). Hyprop user manual. *GmbH München*.

[Van Genuchten, 1980] Van Genuchten, M. T. (1980). A closed-form equation for predicting the hydraulic conductivity of unsaturated soils 1. *Soil science society of America journal*, 44(5):892–898.

[Vandoorne et al., 2012] Vandoorne, B., Beff, L., Lutts, S., and Javaux, M. (2012). Root water uptake dynamics of cichorium intybus var. sativum under water-limited conditions. *Vadose Zone Journal*, 11(3).

[Walker and Richardson, 1991] Walker, C. and Richardson, S. (1991). The use of stable isotopes of water in characterising the source of water in vegetation. *Chemical Geology: Isotope Geoscience Section*, 94(2):145–158.

[Yakir and Sternberg, 2000] Yakir, D. and Sternberg, S. L. (2000). The use of stable isotopes to study ecosystem gas exchange. (July 1999):297–311.

[Yu et al., 2007] Yu, G.-R., Zhuang, J., Nakayama, K., and Jin, Y. (2007). Root water uptake and profile soil water as affected by vertical root distribution. *Plant Ecology*, 189(1):15–30.

A Appendix

A.1 List of symbols

H_2O	Water molecule
Z	Atomic number
N	Neutrons number
A	Mass number
δ	Isotopic composition [‰]
^{16}O ^{18}O	Oxygen stable isotopes
^{2}H ^{1}H	Hydrogen stable isotopes
α	Fractionation factor
α_k	Equilibrium fractionation factor
δ^2H	Stable hydrogen isotopic composition [‰]
$\delta^{18}O$	Stable oxygen isotopic composition[‰]
δ_{pp}	Isotopic composition in precipitation water
R	Concentration ratio between the heavy isotope and the light isotope
R^2	Determinant coefficient for linear regression
T	Temperature [°C]
pF	Logarithm of the absolute value of matric potential in soil water [-log hPa]

A.2 List of acronyms

IRMS	Isotope Ratio Mass Spectroscopy
IRIS	Isotope Ratio Infrared Spectroscopy
EF	Evaporation Front
GMWL	Global Meteoric Water Line
LMWL	Local Meteoric Water Line
RWU	Root Water Uptake
VSMOW	Vienna Standard Mean Ocean Water
RLD	Root Length Density
SWC	Soil Water Content
SIAR	Stable Isotope Analysis in R, statistical mixing model

A.3 Field and lab protocols

Field Protocol

Soil water vapour sampling - Part 1 -

1.	**System preparation** NB : The input pipes can stay in the field between each experiment (are connected).
1.1	Evacuate the condense water, depth by depth for all entries • Disconnect the **input pipes.** • Condemn the entrances of the non-evacuated depths. • Open the synthetic air bottle and install a rate of 1.5 L.min^{-1} with the flow controller during 30 seconds (500 ml.min^{-1} per tube is sufficient)
1.2	• Repeat the operation for each depth (5 times)
2.	**Measurement**
2.1	Install a constant incoming air flow without trapping the water vapour • Connect the **output pipes** at the level of the soil surface. • Install the constant incoming flow at a rate of 1.5 L.min^{-1} during **30 minutes** (100ml.min^{-1} per tube is sufficient)
2.2	• Filling the Dewar with dry ice (up to a third of the thermos height)
2.3	• Connect the input pipes • Connect the output pipes with the traps
2.4	• Open each trap with their inlet valve
2.5	Install a constant incoming air flow with extraction • Install the constant incoming flow at a rate of 1.5 L.min^{-1} during **2 hours** (100ml.min^{-1} per tube is sufficient) NB: - The time is to be adapted according to the quantity of water harvested (function of temperature and humidity). - The minimum critical quantity = 0.2 ml
2.6	• close the trap (closing both valves simultaneously) • Cut the flow (close the bottle)
3.	**Water sampling**
3.1	• Remove the trap from the dewar
3.2	• Immerse the tip of the trap in the dry ice so that the condensed water on the edges is at the bottom of the trap.
3.3	• Melt the water by clasping the trap with your hand and check if enough water is harvested • Disconnect the **output pipes** and remove them from the field
3.4	Follow the Lab protocol

Lab Protocol

Soil water vapour sampling - Part 2 -

3.5	• Wear gloves • Use a hotgun at a temperature of 250°C (high part of the trap) and dry ice at temperature of -80°C (lower part of the trap) in order to create a temperature gradient in the trap. The aim is collect the total amount of water contained in the trap.
3.6	• slowly open the trap
3.7	• Transfer the water into the insert with the help of pipette. This process has to be done relatively quickly to avoid excessive contact with the surrounding air and its associated risk of contamination.
3.8	• Record the number corresponding to the **day** of the experiment and note the **depth**

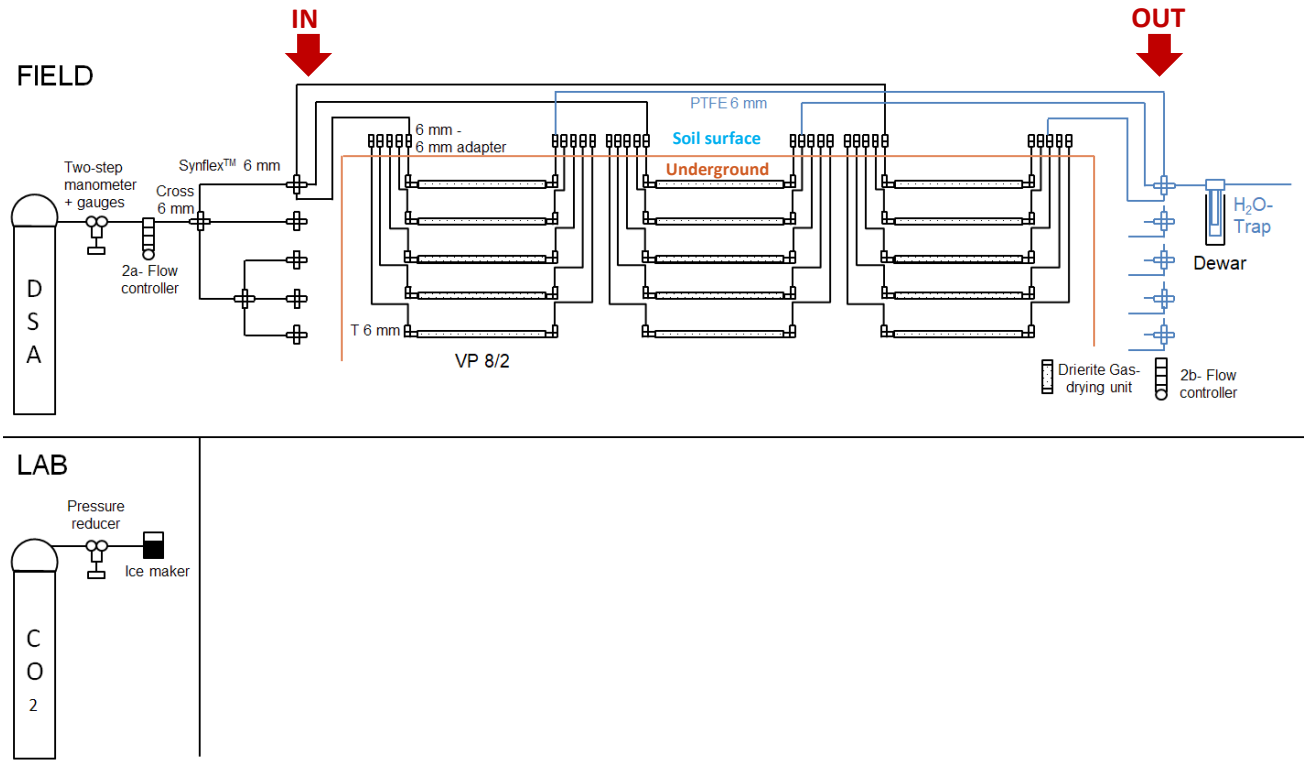

A.4 Calibration equations for the 5TM probes

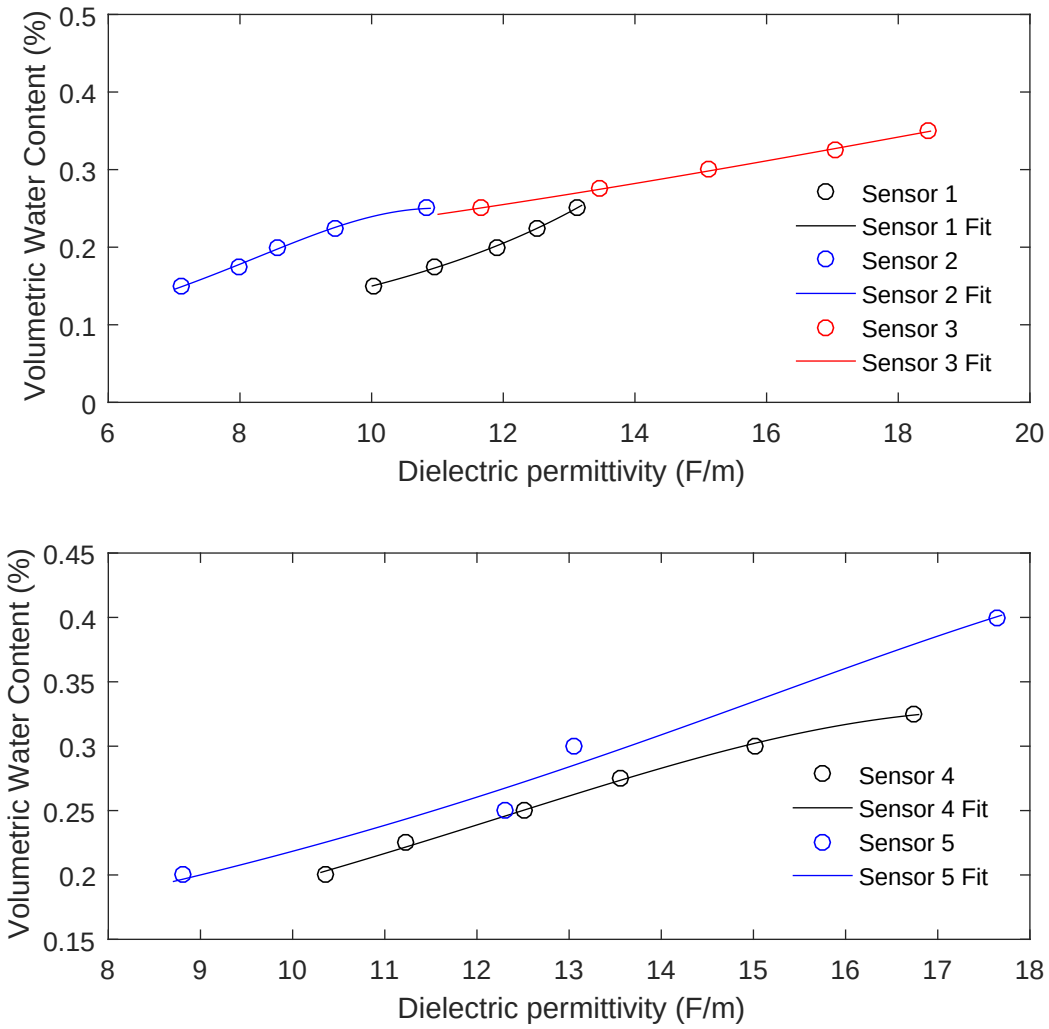

Figure 31: Evolution of the volumetric water content with the dielectric permittivity (ε_0, the raw output data of the sensor) and their respective fit calculated via the model "CurveExpert Basic®").

A.5 Calculation of the p_j's standard deviation

$$\sigma^2_{p_j} = \sum_{k=1}^{5} \left[\left(\frac{\partial p_j}{\partial R_k} \right)^2 \cdot \sigma^2_{R_k} + \left(\frac{\partial p_j}{\partial S_k} \right)^2 \cdot \sigma^2_{S_k} \right], \tag{21}$$

$$\sigma^2_{p_j} = \sum_{k=1}^{5} \left[\left(\frac{\partial p_j}{\partial R_k} \right)^2 \cdot \sigma^2_{R_k} + \left(\frac{\partial p_j}{\partial S_k} \right)^2 \cdot \sigma^2_{S_k} \right] = A + B + C + D \tag{22}$$

$$A = \left(\frac{S_j}{\sum\limits_k R_k S_k} - \left(\frac{R_j \cdot S_j}{\left(\sum\limits_k R_k \cdot S_k \right)^2} \cdot S_j \right) \right)^2 \cdot \sigma^2_{R_j} \tag{23}$$

$$B = \left(\frac{R_j}{\sum\limits_k R_k S_k} - \left(\frac{R_j \cdot S_j}{\left(\sum\limits_k R_k \cdot S_k \right)^2} \cdot R_j \right) \right)^2 \cdot \sigma^2_{S_j} \tag{24}$$

$$C = \sum_{k' \neq j} \left(- \frac{R_j \cdot S_j}{\left(\sum\limits_k R_k \cdot S_k \right)^2} \cdot S_{k'} \right)^2 \cdot \sigma^2_{R_{k'}} \tag{25}$$

$$D = \sum_{k' \neq j} \left(- \frac{R_j \cdot S_j}{\left(\sum\limits_k R_k \cdot S_k \right)^2} \cdot R_{k'} \right)^2 \cdot \sigma^2_{S_{k'}} \tag{26}$$

A.6 Pictures

A.6.1 Tubing installation in the field

Figure 32: Pictures of the tubing installation. Left picture shows the tubes installed 1.3 m deep while the right picture shows the installation at 0.2 m.

A.6.2 Extraction line of the Jülich laboratory

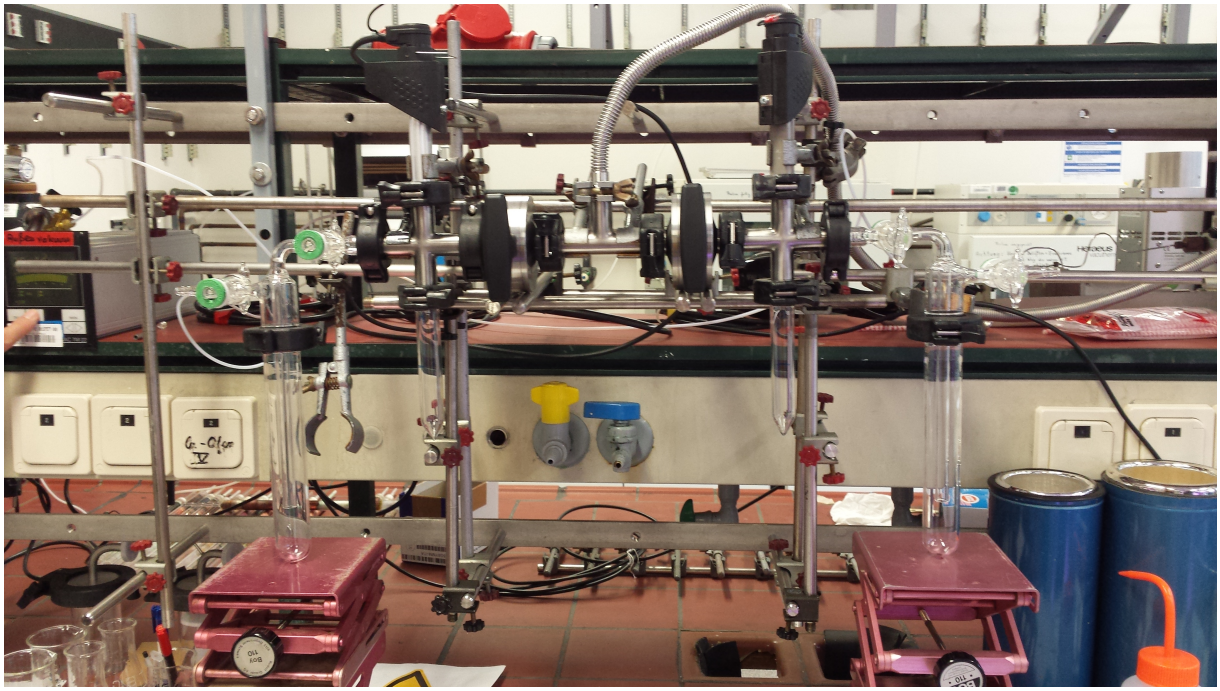

Figure 33: Picture of the extraction line of Jülich Forschungszentrum.

A.7 Output data of the model SIAR

Examples of density curves concerning Date 6 <u>without</u> prior information inserted in SIAR

SD = Standard deviation
n = Run number
∑n = total run number = 30 000
MFV= Most Frequent Value
Rel RWU = Relative Root Water Uptake Proportion

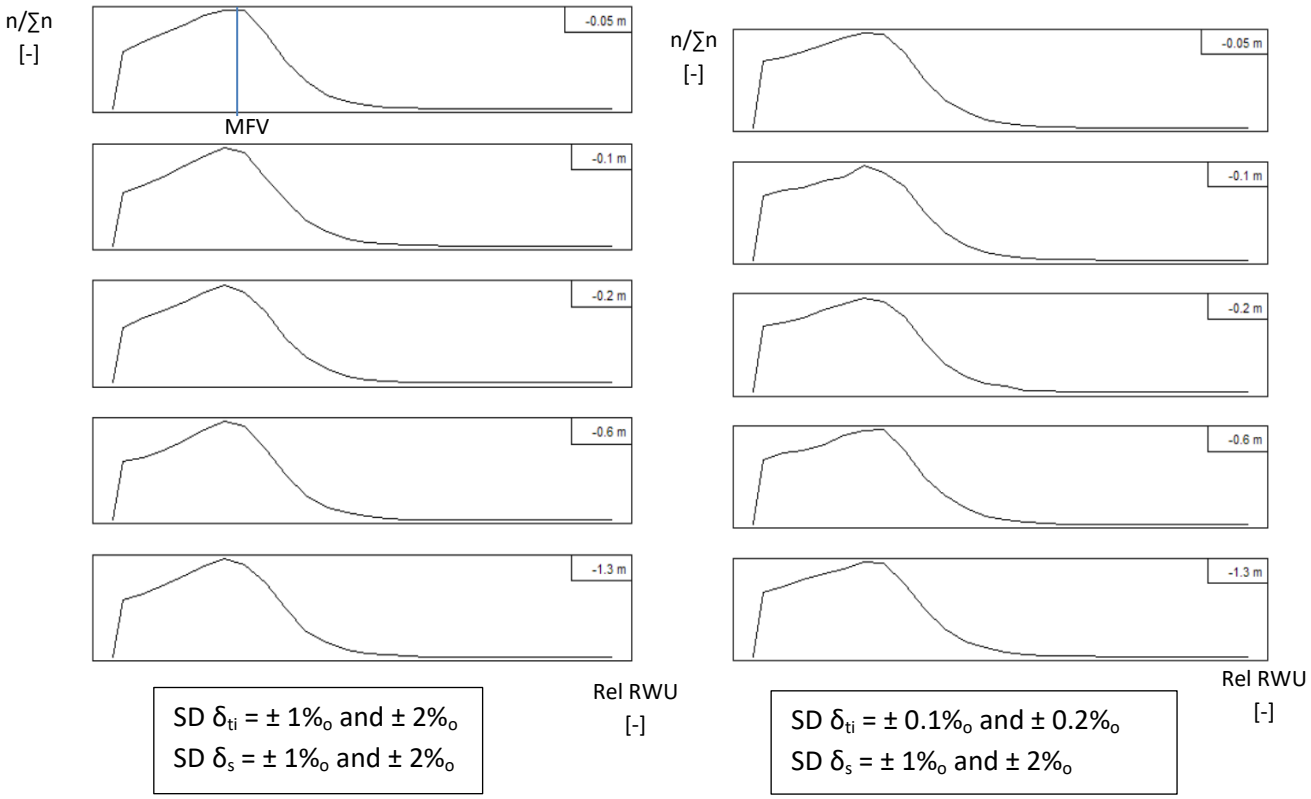

SD δ_{ti} = ± 1‰ and ± 2‰
SD δ_s = ± 1‰ and ± 2‰

SD δ_{ti} = ± 0.1‰ and ± 0.2‰
SD δ_s = ± 1‰ and ± 2‰

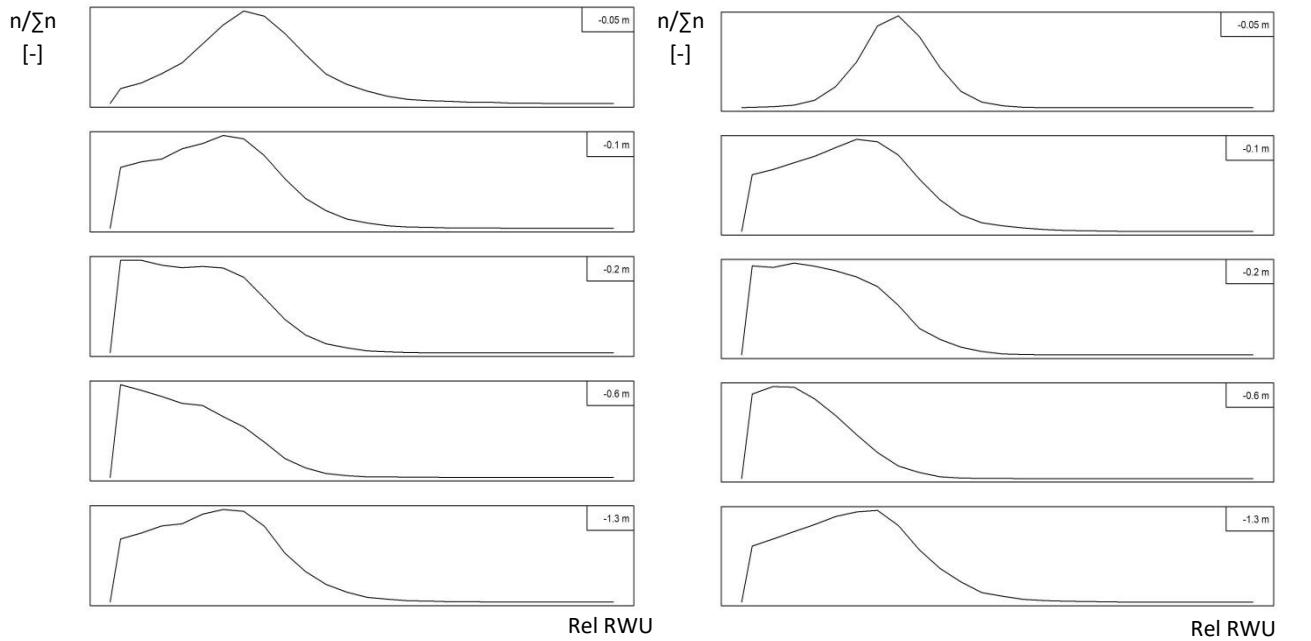

SD δ_{ti} = ± 1‰ or ± 2‰
SD δ_s = analytical errors (± 0.1‰ or ± 0.2‰)

SD δ_{ti} = ± 0.1‰ or ± 0.2‰
SD δ_s = analytical errors (± 0.1‰ or ± 0.2‰)

Density curves concerning Date 6 <u>with</u> prior information inserted in SIAR

(SD = Standard deviation)

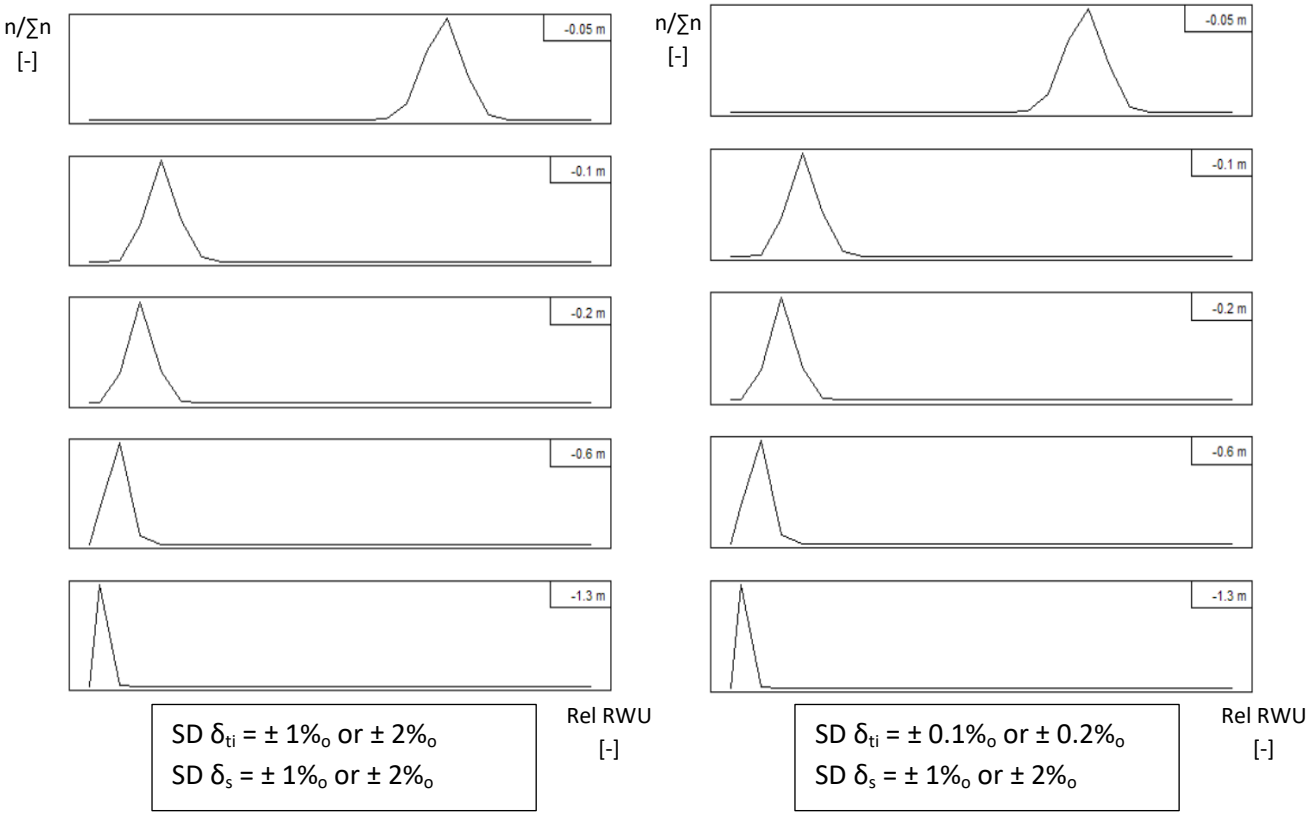

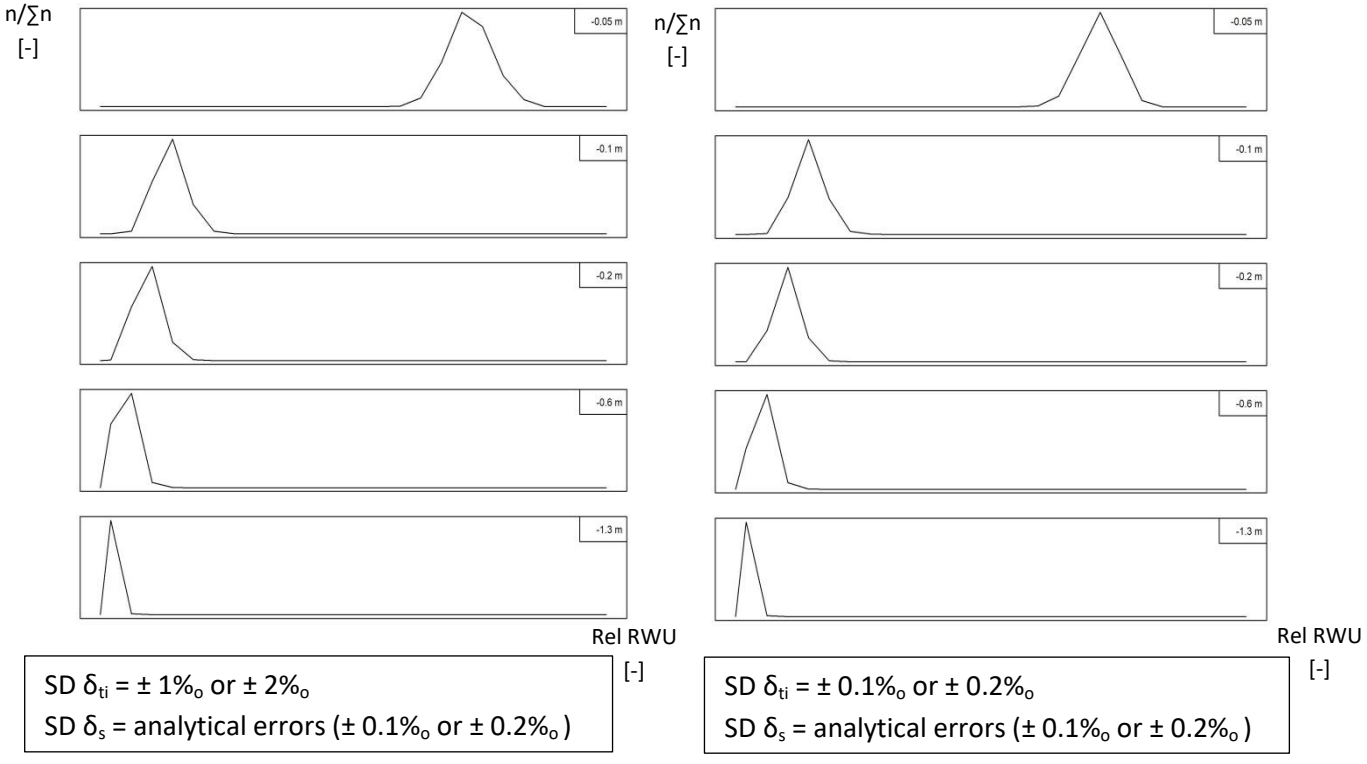

Output data of the model SIAR

1. NO PRIOR information inserted in the model

A. Standard deviations corresponding to :

δ_s = 1 or 2 ‰

δ_{ti} = 1 or 2 ‰

Date	MFV	Min	Max	Source
Date 2	0.22	0.02	0.78	-0.05
	0.22	0.02	0.86	-0.1
	0.22	0.02	0.78	-0.2
	0.22	0.02	0.78	-0.6
	0.22	0.02	0.74	-1.3
Date 3	0.22	0.02	0.82	-0.05
	0.22	0.02	0.86	-0.1
	0.26	0.02	0.86	-0.2
	0.22	0.02	0.90	-0.6
	0.22	0.02	0.82	-1.3
Date 5	0.26	0.02	0.78	-0.05
	0.22	0.02	0.82	-0.1
	0.22	0.02	0.74	-0.2
	0.22	0.02	0.86	-0.6
	0.22	0.02	0.82	-1.3
Date 6	0.22	0.02	0.82	-0.05
	0.22	0.02	0.86	-0.1
	0.22	0.02	0.86	-0.2
	0.22	0.02	0.82	-0.6
	0.22	0.02	0.90	-1.3
Date 7	0.3	0.02	0.94	-0.05
	0.3	0.02	0.94	-0.2
	0.26	0.02	0.90	-0.6
	0.3	0.02	0.94	-1.3

B. Standard deviations corresponding to :

δ_s = 1 or 2 ‰

δ_{ti} = 0.1 or 0.2 ‰

Date	MFV	Min	Max	Source
Date 2	0.22	0.02	0.78	-0.05
	0.22	0.02	0.82	-0.1
	0.22	0.02	0.82	-0.2
	0.22	0.02	0.82	-0.6
	0.26	0.02	0.82	-1.3
Date 3	0.22	0.02	0.82	-0.05
	0.22	0.02	0.86	-0.1
	0.22	0.02	0.86	-0.2
	0.22	0.02	0.90	-0.6
	0.22	0.02	0.82	-1.3
Date 5	0.22	0.02	0.86	-0.05
	0.22	0.02	0.86	-0.1
	0.22	0.02	0.82	-0.2
	0.22	0.02	0.78	-0.6
	0.22	0.02	0.78	-1.3
Date 6	0.22	0.02	0.86	-0.05
	0.22	0.02	0.78	-0.1
	0.22	0.02	0.86	-0.2
	0.26	0.02	0.78	-0.6
	0.22	0.02	0.82	-1.3
Date 7	0.3	0.02	0.90	-0.05
	0.3	0.02	0.90	-0.2
	0.26	0.02	0.90	-0.6
	0.3	0.02	0.94	-1.3

C. Standard deviations corresponding to :

δ_s = analytical errors [$‰_0$]

δ_{ti} = 1 or 2 $‰_0$

Date	MFV	Min	Max	Source
Date 2	0.26	0.02	0.90	-0.05
	0.22	0.02	0.82	-0.1
	0.22	0.02	0.82	-0.2
	0.02	0.02	0.74	-0.6
	0.22	0.02	0.78	-1.3
Date 3	0.30	0.02	0.78	-0.05
	0.06	0.02	0.58	-0.1
	0.10	0.02	0.62	-0.2
	0.22	0.02	0.78	-0.6
	0.22	0.02	0.82	-1.3
Date 5	0.30	0.02	0.86	-0.05
	0.22	0.02	0.74	-0.1
	0.02	0.02	0.74	-0.2
	0.02	0.02	0.74	-0.6
	0.06	0.02	0.78	-1.3
Date 6	0.26	0.02	0.90	-0.05
	0.22	0.02	0.82	-0.1
	0.04	0.02	0.78	-0.2
	0.02	0.02	0.78	-0.6
	0.22	0.02	0.86	-1.3
Date 7	0.34	0.02	0.90	-0.05
	0.06	0.02	0.90	-0.2
	0.26	0.02	0.90	-0.6
	0.06	0.02	0.94	-1.3

D. Standard deviations corresponding to :

δ_s = analytical errors [$‰_0$]

δ_{ti} = 0.1 or 0.2 $‰_0$

Date	MFV	Min	Max	Source
Date 2	0.26	0.02	0.90	-0.05
	0.22	0.02	0.82	-0.1
	0.22	0.02	0.86	-0.2
	0.22	0.02	0.82	-0.6
	0.22	0.02	0.82	-1.3
Date 3	0.26	0.02	0.70	-0.05
	0.22	0.02	0.50	-0.1
	0.22	0.02	0.42	-0.2
	0.02	0.02	0.70	-0.6
	0.22	0.02	0.74	-1.3
Date 5	0.30	0.02	0.70	-0.05
	0.06	0.02	0.50	-0.1
	0.10	0.02	0.42	-0.2
	0.22	0.02	0.70	-0.6
	0.22	0.02	0.74	-1.3
Date 6	0.30	0.02	0.66	-0.05
	0.22	0.02	0.90	-0.1
	0.10	0.02	0.58	-0.2
	0.06	0.02	0.50	-0.6
	0.26	0.02	0.78	-1.3
Date 7	0.34	0.02	0.90	-0.05
	0.26	0.02	0.82	-0.2
	0.22	0.02	0.70	-0.6
	0.22	0.02	0.62	-1.3

1. PRIOR information inserted in the model

A. Standard deviations corresponding to :

δ_s = 1 or 2 $‰_0$

δ_{ti} = 1 or 2 $‰_0$

Date	MFV	Min	Max	Source
Date 2	0.66	0.54	0.82	-0.05
	0.14	0.06	0.26	-0.1
	0.10	0.02	0.22	-0.2
	0.06	0.02	0.14	-0.6
	0.02	0.02	0.06	-1.3
Date 3	0.70	0.50	0.82	-0.05
	0.14	0.06	0.26	-0.1
	0.10	0.06	0.22	-0.2
	0.06	0.02	0.18	-0.6
	0.02	0.02	0.10	-1.3
Date 5	0.70	0.54	0.82	-0.05
	0.14	0.06	0.26	-0.1
	0.10	0.02	0.22	-0.2
	0.06	0.02	0.14	-0.6
	0.02	0.02	0.10	-1.3
Date 6	0.70	0.54	0.82	-0.05
	0.14	0.06	0.26	-0.1
	0.10	0.02	0.22	-0.2
	0.06	0.02	0.14	-0.6
	0.02	0.02	0.10	-1.3
Date 7	0.78	0.62	0.90	-0.05
	0.14	0.02	0.26	-0.2
	0.06	0.02	0.22	-0.6
	0.02	0.02	0.14	-1.3

B. Standard deviations corresponding to :

δ_s = 1 or 2 $‰_0$

δ_{ti} = 0.1 or 0.2 $‰_0$

Date	MFV	Min	Max	Source
Date 2	0.66	0.54	0.82	-0.05
	0.14	0.06	0.26	-0.1
	0.10	0.02	0.26	-0.2
	0.06	0.02	0.14	-0.6
	0.02	0.02	0.10	-1.3
Date 3	0.70	0.50	0.82	-0.05
	0.14	0.06	0.26	-0.1
	0.10	0.06	0.22	-0.2
	0.06	0.02	0.14	-0.6
	0.02	0.02	0.06	-1.3
Date 5	0.70	0.54	0.82	-0.05
	0.14	0.06	0.26	-0.1
	0.10	0.02	0.22	-0.2
	0.06	0.02	0.14	-0.6
	0.02	0.02	0.10	-1.3
Date 6	0.70	0.54	0.82	-0.05
	0.14	0.06	0.30	-0.1
	0.10	0.02	0.22	-0.2
	0.06	0.02	0.14	-0.6
	0.02	0.02	0.10	-1.3
Date 7	0.78	0.62	0.90	-0.05
	0.14	0.02	0.26	-0.2
	0.06	0.02	0.22	-0.6
	0.02	0.02	0.14	-1.3

C. Standard deviations corresponding to :

δ_s = analytical errors [$‰_0$]

δ_{ti} = 1 or 2 $‰_0$

Date	MFV	Min	Max	Source
Date 2	0.70	0.54	0.82	-0.05
	0.14	0.06	0.26	-0.1
	0.10	0.02	0.22	-0.2
	0.06	0.02	0.14	-0.6
	0.02	0.02	0.06	-1.3
Date 3	0.66	0.50	0.78	-0.05
	0.14	0.06	0.30	-0.1
	0.10	0.06	0.26	-0.2
	0.06	0.02	0.18	-0.6
	0.02	0.02	0.10	-1.3
Date 5	0.66	0.54	0.82	-0.05
	0.14	0.06	0.26	-0.1
	0.10	0.02	0.22	-0.2
	0.06	0.02	0.14	-0.6
	0.02	0.02	0.10	-1.3
Date 6	0.70	0.54	0.82	-0.05
	0.14	0.06	0.30	-0.1
	0.10	0.02	0.18	-0.2
	0.06	0.02	0.14	-0.6
	0.02	0.02	0.10	-1.3
Date 7	0.78	0.62	0.90	-0.05
	0.14	0.02	0.30	-0.2
	0.06	0.02	0.22	-0.6
	0.02	0.02	0.14	-1.3

D. Standard deviations corresponding to :

δ_s = analytical errors [$‰_0$]

δ_{ti} = 0.1 or 0.2 $‰_0$

Date	MFV	Min	Max	Source
Date 2	0.70	0.54	0.82	-0.05
	0.14	0.06	0.26	-0.1
	0.10	0.02	0.22	-0.2
	0.06	0.02	0.14	-0.6
	0.02	0.02	0.06	-1.3
Date 3	0.66	0.50	0.78	-0.05
	0.14	0.06	0.26	-0.1
	0.10	0.06	0.22	-0.2
	0.06	0.02	0.18	-0.6
	0.02	0.02	0.10	-1.3
Date 5	0.66	0.54	0.78	-0.05
	0.14	0.06	0.26	-0.1
	0.10	0.02	0.22	-0.2
	0.06	0.02	0.14	-0.6
	0.02	0.02	0.10	-1.3
Date 6	0.70	0.54	0.54	-0.05
	0.14	0.06	0.26	-0.1
	0.10	0.02	0.22	-0.2
	0.06	0.02	0.14	-0.6
	0.02	0.02	0.10	-1.3
Date 7	0.78	0.62	0.90	-0.05
	0.14	0.02	0.26	-0.2
	0.06	0.02	0.22	-0.6
	0.02	0.02	0.14	-1.3